National Library of Canada

Bibliothèque nationale du Canada

Acquisitions and Bibliographic Services Branch

Direction des acquisitions et des services bibliographiques

395 Wellington Street
Ottawa, Ontario
K1A 0N4

395, rue Wellington
Ottawa (Ontario)
K1A 0N4

Your file Votre référence

Our file Notre référence

NOTICE

The quality of this microform is heavily dependent upon the quality of the original thesis submitted for microfilming. Every effort has been made to ensure the highest quality of reproduction possible.

If pages are missing, contact the university which granted the degree.

Some pages may have indistinct print especially if the original pages were typed with a poor typewriter ribbon or if the university sent us an inferior photocopy.

Reproduction in full or in part of this microform is governed by the Canadian Copyright Act, R.S.C. 1970, c. C-30, and subsequent amendments.

AVIS

La qualité de cette microforme dépend grandement de la qualité de la thèse soumise au microfilmage. Nous avons tout fait pour assurer une qualité supérieure de reproduction.

S'il manque des pages, veuillez communiquer avec l'université qui a conféré le grade.

La qualité d'impression de certaines pages peut laisser à désirer, surtout si les pages originales ont été dactylographiées à l'aide d'un ruban usé ou si l'université nous a fait parvenir une photocopie de qualité inférieure.

La reproduction, même partielle, de cette microforme est soumise à la Loi canadienne sur le droit d'auteur, SRC 1970, c. C-30, et ses amendements subséquents.

Canada

UNIVERSITY OF ALBERTA

PREPARATION AND CHARACTERIZATION OF CARBON NITRIDE THIN FILMS

BY

LIAN WAN

A thesis submitted to the Faculty of Graduate Studies and Research in partial fulfillment of the requirements for the degree of master of science

DEP .RTMENT OF PHYSICS

EDMONTON, ALBERTA

SPRING 1995

National Library of Canada

Bibliothèque nationale du Canada

Acquisitions and Bibliographic Services Branch

Direction des acquisitions et des services bibliographiques

395 Wellington Street
Ottawa, Ontario
K1A 0N4

395, rue Wellington
Ottawa (Ontario)
K1A 0N4

Your file Votre référence

Our file Notre référence

THE AUTHOR HAS GRANTED AN IRREVOCABLE NON-EXCLUSIVE LICENCE ALLOWING THE NATIONAL LIBRARY OF CANADA TO REPRODUCE, LOAN, DISTRIBUTE OR SELL COPIES OF HIS/HER THESIS BY ANY MEANS AND IN ANY FORM OR FORMAT, MAKING THIS THESIS AVAILABLE TO INTERESTED PERSONS.

L'AUTEUR A ACCORDE UNE LICENCE IRREVOCABLE ET NON EXCLUSIVE PERMETTANT A LA BIBLIOTHEQUE NATIONALE DU CANADA DE REPRODUIRE, PRETER, DISTRIBUER OU VENDRE DES COPIES DE SA THESE DE QUELQUE MANIERE ET SOUS QUELQUE FORME QUE CE SOIT POUR METTRE DES EXEMPLAIRES DE CETTE THESE A LA DISPOSITION DES PERSONNE INTERESSEES.

THE AUTHOR RETAINS OWNERSHIP OF THE COPYRIGHT IN HIS/HER THESIS. NEITHER THE THESIS NOR SUBSTANTIAL EXTRACTS FROM IT MAY BE PRINTED OR OTHERWISE REPRODUCED WITHOUT HIS/HER PERMISSION.

L'AUTEUR CONSERVE LA PROPRIETE DU DROIT D'AUTEUR QUI PROTEGE SA THESE. NI LA THESE NI DES EXTRAITS SUBSTANTIELS DE CELLE-CI NE DOIVENT ETRE IMPRIMES OU AUTREMENT REPRODUITS SANS SON AUTORISATION.

ISBN 0-612-01661-7

Canada

UNIVERSITY OF ALBERTA
LIBRARY RELEASE FORM

NAME OF AUTHOR: **LIAN WAN**

TITLE OF THESIS: **PREPARATION AND CHARACTERIZATION OF CARBON NITRIDE THIN FILMS**

DEGREE: **MASTER OF SCIENCE**

YEAR THIS DEGREE GRANTED: **1995**

Permission is hereby granted to the University of Alberta to reproduce single copies of this thesis and to lend or sell such copies for private, scholarly or scientific research purposes only.

The author reserves all other publication and other right in association with the copyright in the thesis, and except as hereinbefore provided neither the thesis nor any substantial portion thereof may be printed or otherwise reproduced in any material form whatever without the author's prior written permission.

Lian Wan
10726-85 Ave, #103
Edmonton, Alberta
Canada T6E 2K8

February 16, 1995

UNIVERSITY OF ALBERTA

FACULTY OF GRADUATE STUDIES AND RESEARCH

The undersigned certify that they have read, and recommend to the Faculty of Graduate Studies and Research for acceptance, a thesis entitled **PREPARATION AND CHARACTERIZATION OF CARBON NITRIDE THIN FILMS** submitted by **LIAN WAN** in partial fulfillment of the requirements for the degree of **MASTER OF SCIENCE**

R. F. Egerton

Dr. R. F. Egerton(supervisor)

John Beamish

Dr. J. Beamish

M. Brett

Dr. M. Brett

Ronald PW Lawson

Dr. RPW Lawson

February 16, 1995

ABSTRACT

Carbon Nitride (CN_x) thin films were deposited by carbon-arc evaporation (with and without a bias voltage applied to the substrate) in a low pressure of N_2 or NH_3 gas, and by d.c. and r.f. sputtering in N_2 or a Ar/N_2 mixture. Substrates were cleaved KCl, NaCl, mica and cleaned {100} silicon wafer, held at various temperatures [illegible]om -100°C to 600°C. Transmission electron diffraction (TED) patterns show the film to be mainly amorphous, with no e[illegible]r the existence of the proposed β-C_3N_4 crystalline material. N/C ratios of the as-de[illegible] film, measured from electron energy-loss spectroscopy (EELS), are betwe[illegible]75 depending on deposition conditions. The bonding type is estimated from the fine structure of the carbon K-ionization edge analysis, which gave an sp^2 bonded fraction of more than 100% on most CN_x films, probably due to the existence of sp bonds and charge transfer between carbon and nitrogen atoms. This fraction tended to increase as the nitrogen content increased. After annealing at 800°C, up to 75% of the nitrogen was released, which suggests that most of the carbon-nitrogen bonds are weak.

ACKNOWLEDGEMENTS

I wish to express my sincere gratitude to Dr. Ray Egerton, my supervisor, for his support and guidance to this project, for his encouragement and patience throughout the course of this work, and for his careful editing of the manuscript. Without him, this thesis could not be finished.

I am deeply indebted to a host of people involved in every aspect of this study. Dr. Craig Bennett, Dr. Shang-Cong Cheng and Dr. Kaikee Wong were very helpful at various stages in specimen preparation and results analysis.

I would like to thank Mr. John Malinski and Mr. Don Mullin for their capable assistance with the technical problems involved with deposition and microscopy.

Finally, I thank my wife, Xiumei, for her continued support and enthusiasm in all my endeavour.

TABLE OF CONTENTS

CHAPTER **PAGE**

1 Introduction to CN_x thin films 1

1.1 Theoretical prediction 2

1.2 Synthesis of carbon nitride 5

2 Preparation of CN_x thin films 10

2.1 Carbon arc-discharge evaporation 10

2.1.1 Carbon arc discharge evaporation without a bias on the substrate 12

2.1.2 Carbon arc discharge evaporation with a bias on the substrate 12

2.2 Reactive magnetron sputter deposition 13

2.3 Working gases and pressure 16

2.4 Substrate type and temperature 16

3 Instrumentation and Analysis Methods 20

3.1 The analytical electron microscope (AEM) -- JEOL2010 20

3.2 EELS system 22

3.2.1 Low loss spectrum and K-shell loss spectrum 24

3.2.2 Thickness of the films 26

3.2.3 Plasmon energy 28

3.2.4 Nitrogen/Carbon ratio of the CN_x films 29

3.2.5 Bond structure 30

3.3 Energy dispersive x-ray spectroscopy (EDX) 37

4 Results and discussions 40

4.1 Nitrogen/carbon ratio 42

4.1.1 Effect of electron beam irradiation 43

4.1.2 Effect of annealing 45

4.1.3 Effect of substrate temperature 46

4.1.4 Effect of other sputtering parameters 48

4.2 Bond structure 49

4.2.1 The dependence of R_{sp2} on N/C ratio x and substrate temperature 54

4.2.2 Effect of annealing 56

4.2.3 The dependence of R_{sp2} on other sputtering parameters 56

4.3 Plasmon Energy 58

4.4 The Occurrence of Crystallites 60

5 Conclusions 65

Bibliography 66

Appendix 69

LIST OF TABLES

TABLE **PAGE**

1 Lattice constants and crystalline coordinates of predicted β-C_3N_4 3

2 Collection angles for several objective apertures 26

3 N/C ratio x of CN_x thin films deposited at
different conditions before and after annealing to 800°C 43

4 Dependence of N/C ratio x on sputtering conditions 48

5 Comparison of two plural scattering removing methods 49

6 The d-spacings(nm) of the crystallite found in CN_x film deposited on silicon
substrate at 500°C, theoretical calculation of β-C_3N_4, silicon, and graphite 63

LIST OF FIGURES

FIGURE	PAGE
1 Structure of predicted β-C_3N_4	4
2 Apparatus of carbon arc discharge evaporation	11
3 Installation of the sputter system for CN_x films deposition	15
4 The dependence of the deposition rate of CN_x films on substrate temperature when deposited on mica with 40 watts sputtering power	19
5 The AEM system at the Department of Physics, University of Alberta	21
6 The Gatan 666 PEELS system	23
7 Typical EELS of CN_x film	25
8 Low loss spectrum of carbon film (after deconvolution) and its dielectric constant	32
9 Fit of the π peak with a Lorentzian	35
10 EDX spectrum of CN_x thin film (by sputtering, x=0.4)	38
11 TEM image and diffraction pattern of a CN_x film deposited by DC-sputtering in 20 mTorr N_2, at 40 watts power on KCl substrate	41
12 The change of N/C ratio of an DC sputtered CN_x thin film under electron beam irradiation	44
13 N/C ratio x depends on substrate temperature (Deposition condition: d.c. sputtering in 20 mTorr N_2, at 40 watt power on mica substrate)	46
14 CN_x replica of evaporated KCl surface	47
15 Comparison of carbon and nitrogen K-shell loss fine structure	53

16 Dependence of R_{sp2} on N/C ratio x 55

17 Dependence of R_{sp2} on substrate temperature 55

18 Effect of annealing on R_{sp2} 57

19 Relationship of R_{sp3}/R_{sp2} and plasmon energy 59

20 TEM image and diffraction pattern of a CN_x film containing crystallite 61

21 Selected area EELS of the crystallite found in CN_x film deposited on silicon at 500°C 64

Chapter 1 INTRODUCTION TO CN_x THIN FILMS

Carbon thin films can be produced by various deposition techniques, covering a wide range of properties and applications. Amorphous carbon films (α-C) deposited by evaporation by an electron beam or carbon discharge arc (Bradley,1954) or by sputtering (McLintock and Orr 1973) are smooth, strong and conductive. They have been used as specimen supports, replicas and conductive coatings for scanning electron microscope samples. Diamond films are formed by various chemical vapor deposition (CVD) and physical vapor deposition (PVD) processes (Davis 1992). Diamond-like-carbon (DLC) films are produced by laser ablation (Davanloo, 1990), filtered arc deposition (Berger 1988) and ion beam deposition (Weissmantel, 1979). Hydrogenated DLC (α-C:H) can be prepared by glow discharge (Meyerson and Smith, 1980) or by plasma enhanced CVD (Dworschak 1990). The hydrogen atoms in the film will saturate the dangling bonds of carbon atoms, which avoids the forming of double and triple bonds, hence more sp^3 character will show. All these diamond films, DLC films, and α-C:H films have physical, chemical and mechanical properties similar to those of crystalline diamond. They are excellent candidates as wear-resistant coatings.

The study of nitrogen incorporation in α-C film began in 1982 when Jones and Stewart (1982) incorporated nitrogen into α-C:H films by plasma decomposition of methane and N_2. The nitrogen content in the film was around 5%. They found the electrical conductivity increases as the partial pressure of dopant gas N_2 during film growth increases. Infrared absorption spectroscopy revealed the existence of C=N and C≡N bonds (Han and Feldman 1988). Naturally one can compare the structure of nitrogen doped α-C film with the well understood compound silicon nitride. Then some potential useful mechanical and electrical properties like extremely high hardness and semiconductivity are predicted, which motivated more research interest in this new compound, carbon nitride. Such studies may also be helpful to understanding of interstellar dust since nitrogenated carbon is likely to exist in outer space (Han and Feldman, 1988).

1.1 Theoretical prediction

In 1989, a complex structure for a C-N solid, based on the β-Si_3N_4 structure with C substituted for Si, was described (Liu and Cohen, 1989) (Fig. 1). This structure can be thought of as a complex network of CN_4 tetrahedra that are linked at the corners (space group is $P6_3/m$). The atomic coordination suggests sp^3 hybridization of the carbon atoms and sp^2 hybridization on the N atoms. Although there is no reason to believe this is the lowest energy structure, the moderately large cohesive energy of 5.8eV per atom suggests that there

is a good chance that β-C_3N_4 is at least a metastable structure. The calculated bulk modulus of β-C_3N_4 is 4.27 Mbar, which is very close to that of diamond 4.43Mbar, suggests that the hardness of β-C_3N_4 would be also close to that of diamond. The predicted velocity of sound in β-C_3N_4 of about 1.1×10^6 cm/s suggests a good thermal conductivity. The good agreement of the structural properties of β-Si_3N_4 calculated by the same method with experimental values gives support to the prediction of β-C_3N_4 (Liu and Cohen, 1990). All the calculated lattice constants and crystalline matrix are worked out and given in table 1.

Table 1 The calculated lattice constants and crystalline coordinates of β-C_3N_4.

Type: Hexagonal

a=b=0.644nm , c=0.241nm, $\alpha=\beta=90^\circ$, $\gamma=120^\circ$

Coordinates: x	y	z	occupation	elements
0.500	0.667	0.250	100%	N
-0.500	-0.667	-0.250	100%	N
0.321	0.025	0.250	100%	N
-0.320	-0.025	-0.250	100%	N
-0.025	0.296	0.250	100%	N
0.025	-0.296	-0.250	100%	N
-0.296	-0.320	0.250	100%	N
0.296	0.321	-0.250	100%	N
0.172	-0.231	0.250	100%	C
-0.171	0.231	-0.250	100%	C
0.231	0.403	0.250	100%	C
-0.231	-0.403	-0.250	100%	C
-0.403	0.171	0.250	100%	C
0.403	0.172	-0.250	100%	C

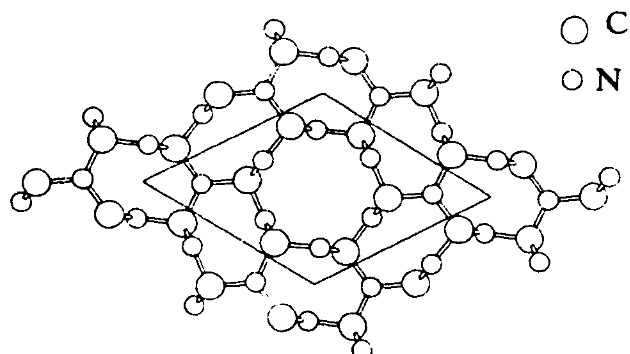

(a) The proposal structure of β-C_3N_4 in the a-b plane. The c-axis is normal to the page. Half of the atoms are located in the z=-c/4 plane, the other half are in z=c/4 plane.

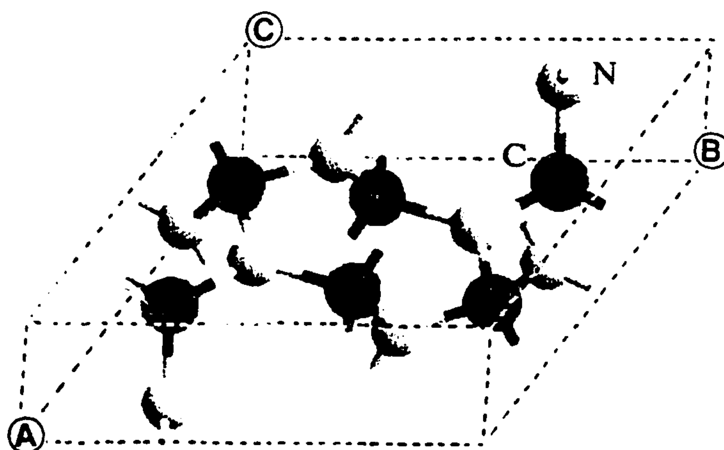

(b) Computer model of β-C_3N_4 displays a single unit cell.
Fig. 1. Structure of predicted β-C_3N_4

Most recently Liu and Wentzcovitch (1994) did some calculations on proposed C_3N_4 crystallites with different structures; one is zinc-blende-like cubic, the other is graphite-like rhombohedral. Both phases have moderately large cohesive energies and are metastable. The bulk modulus of the cubic one is 4.27 Mbar, again close to that of diamond. The graphite-like structure cc tains sp^2 bonds. Their work suggests that carbon nitride may exist in different stable phases.

1.2 Synthesis of carbon nitride

Liu and Cohen's prediction greatly stimulated researchers to synthesize carbon nitride (CN_x). Tens of methods were tried in less than 4 years. Those methods could be classified into:

1) High pressure synthesis, including shock wave co npression (Wixom, 1990) and high pressure pyrolysis (Maya, Cole and Hagaman, 1991). The shock wave compression conditions were sufficient to produce diamond from graphite, as well as to transfer hexagonal boron nitride into the cubic form, but only diamond crystallites were found in the resulting residue by X-ray diffraction (XRD) or Raman measurements. CN_x prepared by pyrolysis of several organic compounds with high nitrogen content (in a medium-pressure closed vessel) showed little nitrogen loss, but were amorphous with relatively low density. There was no evidence for the existence of sp^3 hybridization carbon.

2) Ion beam deposition (IBD). The deposition was done by a single carbon ion beam in nitrogen ambient (single beam) (Mansour and Ugolini, 1993) or by fast-switched carbon and nitrogen sources (dual-beam) (Marton et al, 1994). Essentially filtered cathodic vacuum arc deposition (Veerasamy et al, 1993) is IBD with a special way to generate carbon ion beam. The composition of the products depends on the ion energy and the nitrogen partial pressure in the ambient or the arrival ratio on the substrate of the two ion beams. By single beam deposition, the nitrogen/carbon ratio x is around 0.1. By dual-beam deposition, x could be as high as 0.7, but lower than that of β-C_3N_4, namely 1.33. All the as-deposited films were amorphous.

3) Chemical vapor deposition (CVD). Similar to the deposition of hydrogenated carbon film, N-containing α-C:H film can form by plasma enhanced CVD in the mixture of organic gas (C_6H_6) and nitrogen (Kalish et al., 1991). It is not easy to increase the nitrogen concentration by CVD ($x<0.1$). The results agree with the early research on nitrogen doping of α-C:H films, ie. the electrical conductivity increases and the density of defect states decreases as nitrogen content increases (Lin et al, 1991).

4) Plasma enhanced and ion assisted evaporation. Excited nitrogen species (20-30eV) were generated by electron cyclotron resonance (ECR) plasma to incorporate them in carbon evaporated by electron beam on pure graphite (Bousetta, 1994). From both Rutherford backscattering (RBS) and X-ray photoelectron spectroscopy (XPS) measurements, the

nitrogen concentration in as-deposited film was in the range of 24%-48%, depending on the nitrogen partial pressure in the ECR source. A well resolved Raman spectroscope peak at 1275 cm^{-1} and the shift of C 1s binding energy to that of diamond suggest the formation of a fourfold coordinated (sp^3) CN_x film. Another method is nitrogen ion bombardment during electron beam evaporation of graphite (Fujimoto, F. and Ogata, K. 1993). The reported x is in the range of 0.5-5 depending on the arrival ratio of carbon atoms and nitrogen ions. Since these results were obtained from XPS, a surface analysis technique, the incrediblly high x may be only from surface absorption. More than one Auger electron spectroscopy (AES) depth profile on CN_x film prepared by other methods show lower nitrogen content inside the film than at the surface (Chen, et al. 1992, Marton, et al. 1994). Further investigation is necessary on the ion assisted evaporated films.

5) Nitrogen implantation into solid carbon. The aim of nitrogen implantation is to study the possible bond structures of C-N. XPS results of N implanted graphite show that there are three different nitrogen binding energies, indicating three different nitrogen bonding states. Among them, one is not stable against heat (Hoffman et al, 1993). Optical absorption and dc electrical conductivity measurements on nitrogen-implanted DLC reveal the transformation of DLC (sp^3 dominated) film to a conductive amorphous carbon (sp^2 dominated) film due to the incorporation of nitrogen (Doll, et al. 1994).

6) Reactive sputtering. r.f. or d.c. sputtering of a graphite target in nitrogen or a mixture of nitrogen and argon are the most common ways in producing CN_x thin films. In most cases

(Torng, et al. 1990, Chen et al. 1993, Nakayama, et al, 1993) the products are primarily amorphous, with x ranging from 0.1-0.5. Results from different groups using different analysis methods such as XPS, AES, EELS, infrared spectra and Raman spectra suggest the existence of different C-N bonds, which shows that CN_x is a more complicated system than pure carbon. In two recent experiments crystalline CN_x was reported. One deposition (Yu, et al, 1994) used r.f. sputtering, the other (Sjostrom, et al 1994) used d.c. sputtering, but both were in pure nitrogen gas and onto a heated (100) silicon substrate. The CN_x crystallites obtained by Sjostrom and colleagues were uniform and homogeneous with an interfacial layer of amorphous CN_x (4nm in thickness) adjoining the substrate. The N concentration was about 25%. From electron diffraction, the d-spacings were close to those of the turbostratic structure of carbon (t-C) and boron nitride (t-BN) described by Ning et al.(1990), but far away from the predicted values of β-C_3N_4 . Obviously it is not the proposed crystalline β-C_3N_4. Yu et al.'s CN_x crystallites were grains of 0.5um in diameter, distributed near the film/substrate interface and embedded in the polymeric matrix. They were estimated to occupy less than 5% of the film volume. The authors believed that what they obtained was β-C_3N_4 since there are some matches between the calculated d-spacings of β-C_3N_4 and the experimental values. However the average N concentration was only 30% and other d-spacings did not match with β-C_3N_4.

7) Laser ablation. The first group to claim the successful synthesis of crystalline β-C_3N_4 (Niu, Lu and Lieber, 1993) used pulsed laser ablation of graphite targets combined with an intense atomic nitrogen source. The RBS analysis showed that up to 40% nitrogen could be

incorporated. Small crystallites with grain size < 10 nm were found by transmission electron microscopy (TEM). Some of the d-spacings obtained from electron diffraction pattern match with some of the calculated values of β-C_3N_4. But some of the predicted intense rings were missing, which raises questions about the real identity of the material.

Although it is hard to say whether C_3N_4 has been synthesized, these efforts have already brought some valuable applications. Amorphous CN_x film is very hard, and could be a good protective coating for rigid magnetic storage disks (Yeh, et al 1993). The life time of charge stripper foils made by carbon nitride is about 60 times longer than that of conventional carbon strippers (Sugai et al, 1991).

Chapter 2 PREPARATION of CN_x THIN FILMS

2.1 Carbon arc discharge evaporation

The apparatus for arc discharge evaporation of carbon is illustrated in figure 2. The 0.5 cm diameter carbon rods are supported by two aluminum holders which are fixed onto two pieces of stainless steel. The stainless steel pieces work as springs to keep the carbon rods in contact. One of the contact ends is very sharp, the other has a flat slope. A newly cleaved NaCl or KCl substrate is placed 8cm below the contact point. The chamber was pumped down to 7×10^{-6} torr by a diffusion pump. The arc discharge power supply is an a.c. transformer with voltage range of 4 volts-100 volts and current range of 0 amp-300 amps. A discharge arc will be generated at the contact when the current reaches 20Amp and evaporates the sharp end of carbon rod. Amorphous carbon film will be deposited on the substrate, which can be used as reference in later analysis. The substrate was not heated. In order to avoid heating the substrate from the arc, we manually switched on the arc power for 1 second in every 20 seconds. The effective deposition rate depends on the arc current; a typical value is 80nm/minute.

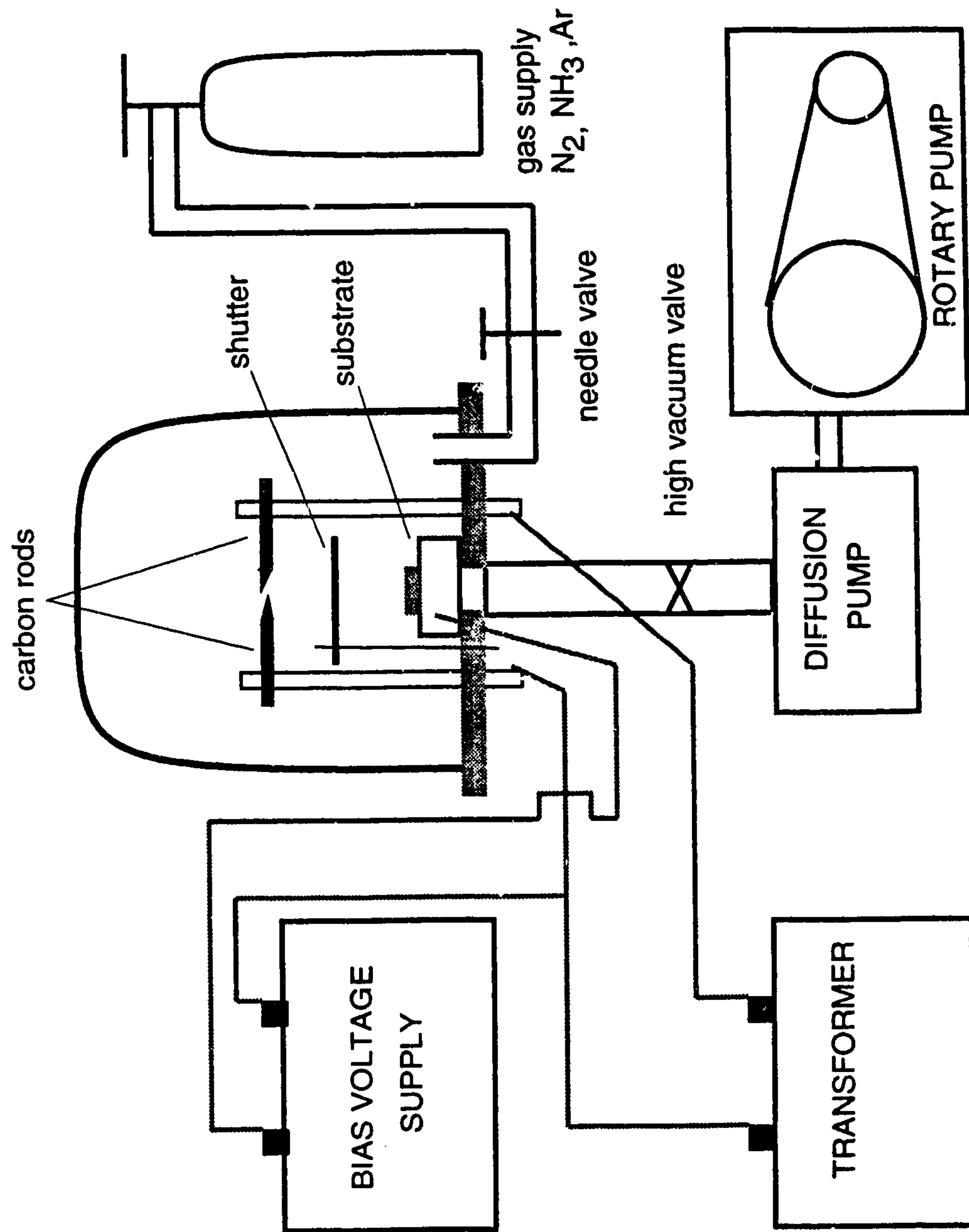

Fig. 2 Apparatus for carbon arc discharge evaporation

2.1.1 Carbon arc discharge evaporation without a bias on the substrate

First we tried to deposit CN_x films directly in N_2 ambient with the above apparatus. After the chamber was pumped down to 10^{-6} torr, pure nitrogen gas (99.998%) was let in through a leak valve to a pressure of 0.05 torr. The arc current was set to 20amps. The deposition rate of the CN_x films at 0.05 torr pressure was only 20nm/minute, about a quarter of that in high vacuum.

Another ambient gas we tested was NH_3. NH_3 should be better for incorporation of nitrogen in carbon since it is more active chemically than N_2. The problem is that there is a chance for hydrogen incorporation into the film, which may change the structure and properties of CN_x film.

Pure Ar was used as a working gas in deposition for comparison of pure carbon films and CN_x films .

2.1.2 Carbon arc discharge evaporation with a bias on the substrate

The products from arc evaporation include mainly carbon clusters and atoms, a small fraction of C^+, C^{2+} ions and electrons. The energy of the deposited particles is very important in determing the bond structure of the film. A bias between the carbon rods and an electrode under the substrate was applied to change the ions' and electrons' energy and

to generate more ions and electrons. The bias can easily generate a pulsed arc between the carbon rods and substrate electrode when it is above 150 volts and the pressure is about 0.05 torr, since it ionizes some of the ambient gas molecules. The interval between each pulse was a couple of seconds. During deposition, this arc or discharge plasma glow can last as long as the carbon arc power supply is on. The current of the glow could reach 100mA when the substrate was connected to the anode, and the carbon rods were connected to the cathode. Conversely the current is only 25mA. The current is mainly determined by the electrons, due to their tiny mass. When the substrate was the anode, the initial velocity of electrons is in the direction of acceleration, producing a larger current; otherwise they are in opposite directions, producing a smaller current .

The depositions were performed in N_2, NH_3 and Ar. There is no significant change of deposition rate with positive, negative bias or zero bias, if the carbon arc current is the same. The reason is that the deposition rate is limited by the mean free path of the carbon atoms, ions, and clusters, which is much shorter than the distance between the source and the substrate.

2.2 Reactive magnetron sputter deposition

Figure 3 show the sputter system we used. The heart is a simple diode magnetron sputtering cathode manufactured by ANGSTROM SCIENCES, which can operate at 0.5 to 200 mtorr with maximum sputtering power of 600 watts. The target is a 2" pyrolytic graphite disc of

99.999% purity. Background pressure of 6×10^{-7} torr can be reached with the CRYO-TORR (R) 8 cryopump (made by CTI-CRYOGENICS). Pure N_2 (99.998%) and Ar (99.999%) cylinders are connected to the vacuum chamber through flow controllers and gauges. The operating pressure and gas flow can be adjusted separately with the combination of the flow controller and the high vacuum valve connected to the cryopump. The substrate stage is equipped with water cooler and electrical heater. With a programmable OMEGA CN2041 profile controller, the substrate stage can be held at any temperature from 20°C to 800°C. The substrate is stuck to the stage with silver paint in order to keep good thermal contact.

The r.f. power supply is RFPP RF5S; the maximum output power is 300 watts, the rf frequency is 13.56MHz. The d.c. sputtering power supply is L. M. SIMARD TS/2 ; the maximum output voltage is 1500 volts, the maximum current is 2.5 Amp. Since graphite is a good conductor, there should be no important difference between r.f. sputtering and d.c. sputtering.

In the plasma, the nitrogen is in the form of ions; the sputtered carbon is in the form of atoms. The particles' energy is 1 to 2 orders of magnitude higher than that of evaporation, giving higher possibility of combining for nitrogen and carbon.

A typical deposition rate at room temperature when the substrate was about 6 cm away from the target was 1 nm/minute.

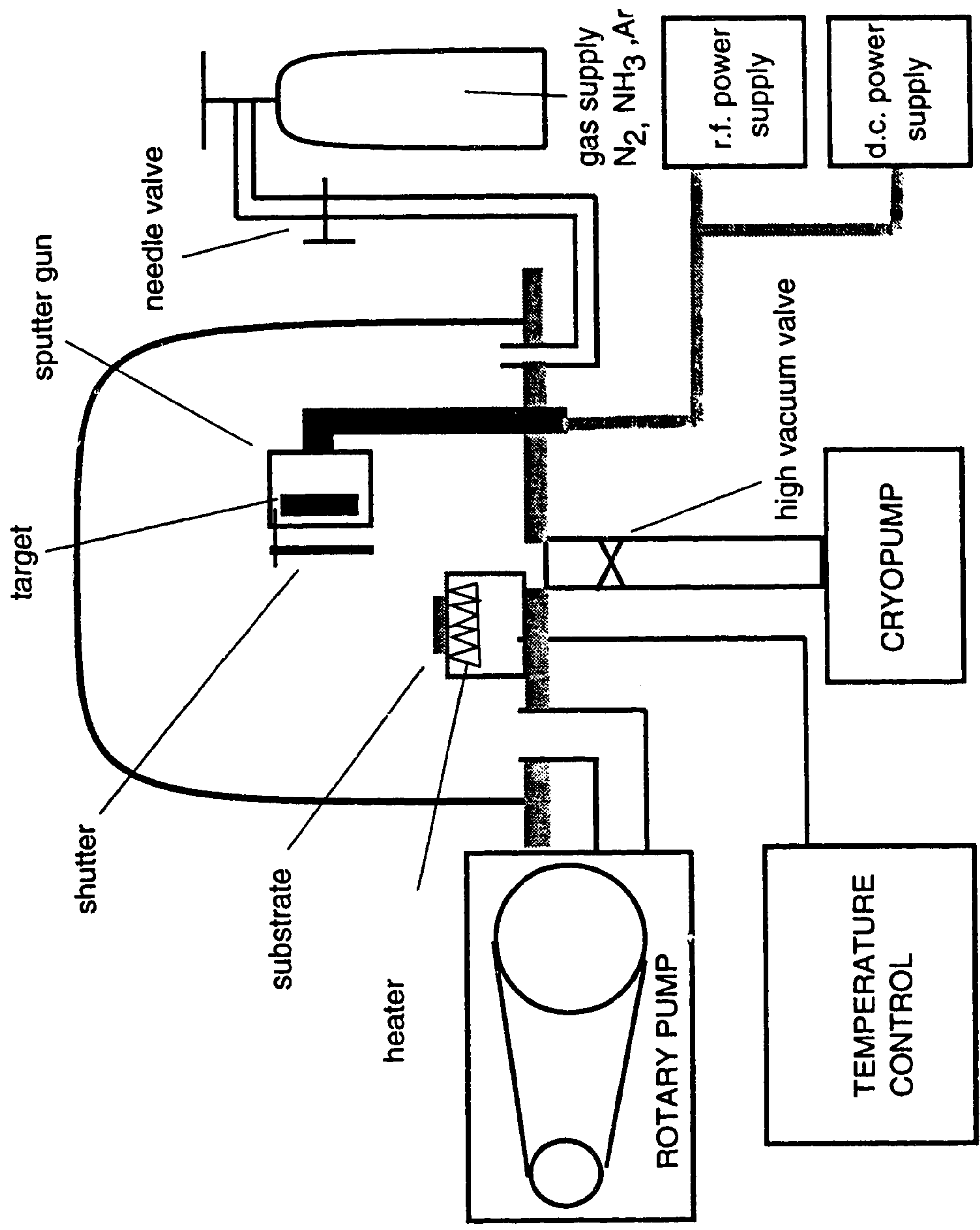

Fig. 3. Installation of the sputter system for CN_x films deposition

2.3 Working gas and pressure

N_2, NH_3, Ar and mixture of Ar and N_2 were used as working gases during sputtering. Although the deposition rate will not change that much because of the sputtering universality, i.e. all materials have sputtering yield close to 2, the composition and the bond structure of the deposited films may be affected by the working gas.

Similar to arc discharge evaporation, increasing the working pressure reduces the deposition rate significantly.

2.4 Substrate type and temperature

The advantages of KCl or NaCl as a substrate are that they are very easy to cleave in order to get a clean surface and that they dissolve in water quickly, leave the CN_x film floating on the surface of water, which is good for making a TEM sample.

It is necessary for crystalline thin film growth that the surface atomic mobility be high enough and that the substrate have the proper structure. When we raise the substrate temperature to improve the surface atomic mobility we also create some problems: NaCl and KCl will be evaporated. When the substrate temperature is 500°C, the deposited CN_x film gets contaminated because the strong diffusion of substrate elements. When it is above

600°C, no film will be deposited on the substrate.

Mica could be a good candidate as a substrate for the deposition of β-C_3N_4 thin film. It can be cleaved easily to obtain a clean surface, it is stable at high temperature (up to 600°C) and some of its lattice constants are close to those of predicted β-C_3N_4. Although it is very difficult to separate thin CN_x films from mica when deposited at room temperature, the adhesion of CN_x films deposited at high substrate temperature is very poor. The films can be removed by the surface tension of water. By careful cleavage, it is also possible to get a small piece of CN_x film on the edge of the mica substrate.

Another suitable substrate is silicon (100), which has most of the advantages of mica, but it is difficult to get a contamination-free surface. Usually dilute HF is necessary to etch away the organic contamination (Bousetta, et al 1994). Sometimes in-situ reverse sputter-etching in argon plasma is applied to remove surface oxides (Li, et al 1993).

One more problem of silicon as a substrate is that it is very hard to separate the CN_x from it. One way to separate them is grinding the CN_x film, suspending the resulting particles in MeOH and then depositing the suspension onto the TEM grids (Niu, Lu, and Lieber, 1993). Another is backpolishing and etching the silicon substrate until a small hole is formed (Yu, et al 1994). The CN_x film will show on the edge of the hole. Both methods are time-consuming and difficult to control.

Before each deposition, we cleaned the silicon substrate by an ultrasonic bath in acetone for 40 minutes followed by 1 hour in situ heating at 500°C in high vacuum. After several tries, we found that a mixture of dilute HF and HNO_3 is an ideal solution for the purpose of separating the film from substrate. At the content around HF:HNO_3:H_2O = 1:9:14, the CN_x films will be removed from the silicon substrate in seconds without any noticeable damage. The films were transferred to distilled water then put onto TEM grids.

As the substrate temperature increases, the deposition rate drops (Fig. 4). At 500°C, the rate is about 0.5 nm/minute (on mica), half of the value at room temperature. At 600°C, it is only 0.1 nm/minute. We also used a heavy metal block, which was transferred to the substrate stage immediately after soaking in liquid nitrogen for an hour to cool down the substrate during deposition. The temperature could be kept below -100°C for more than an hour. The deposition rate in this case is 1.5 nm/minute. The deposition rate varied a little on different substrates.

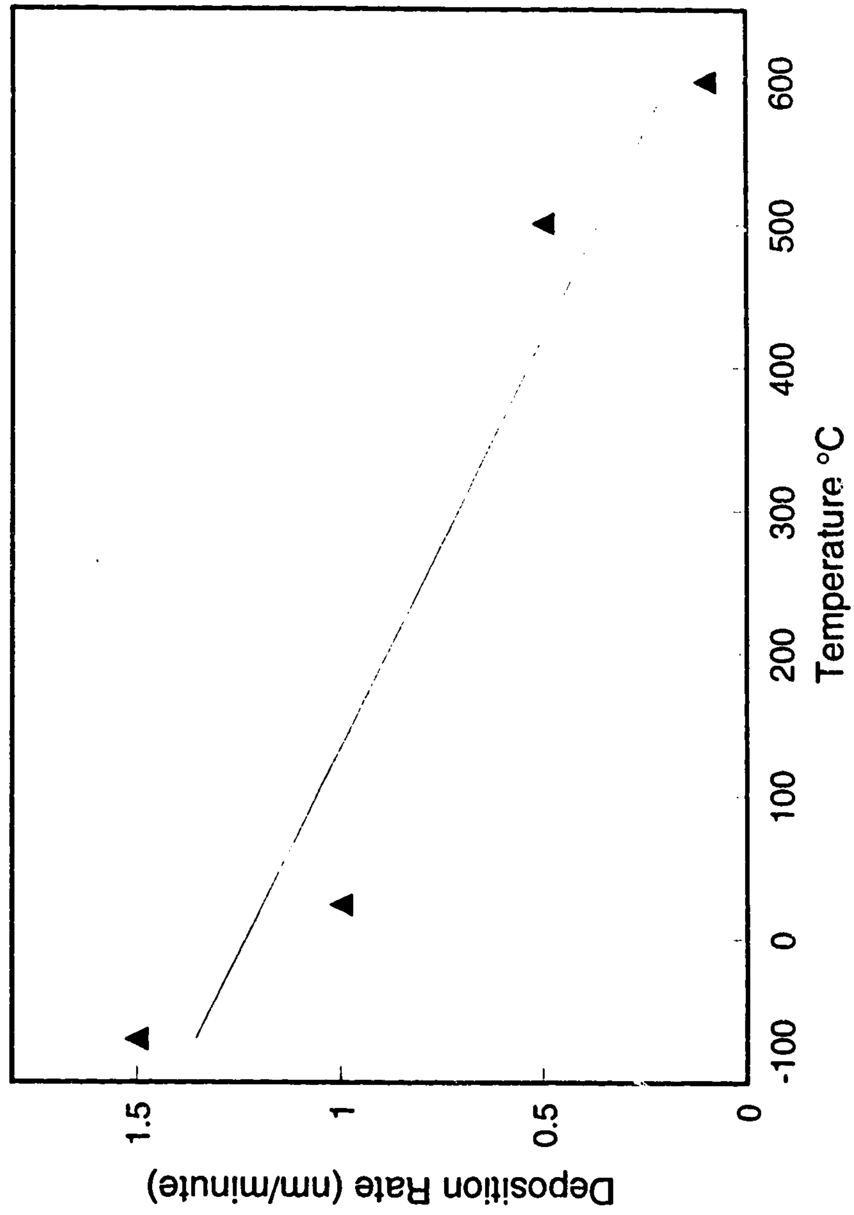

Fig4. The dependence of the deposition rate of CN_x films on substrate temperature when deposited on mica with 40 watts sputtering power

Chapter 3 INSTRUMENTATION AND ANALYSIS METHODS

3.1 The analytical electron microscope (AEM) -- JEOL-2010

The JEOL-2010 transmission electron microscope at the Department of Physics, University of Alberta is shown in figure 5. Its accelerating voltage can be as high as 200kV,which is good for examining of thick specimens. Its magnification is adjustable from 2000 to 1500000 times. The point resolution is better than 0.2nm when fitted with the high-resolution polepieces. Being a ultrahigh resolution analytical electron microscope, the JEOL-2010 is also able to form a sub-nanometer probe for electron-diffraction and microanalysis applications. This TEM is equipped with a Noran energy-dispersive x-ray (EDX) spectrometer and a Gatan 666 electron energy-loss spectroscope (EELS). Along with high resolution TEM images and electron diffraction patterns, this AEM system is a powerful instrument for the study of thin specimens.

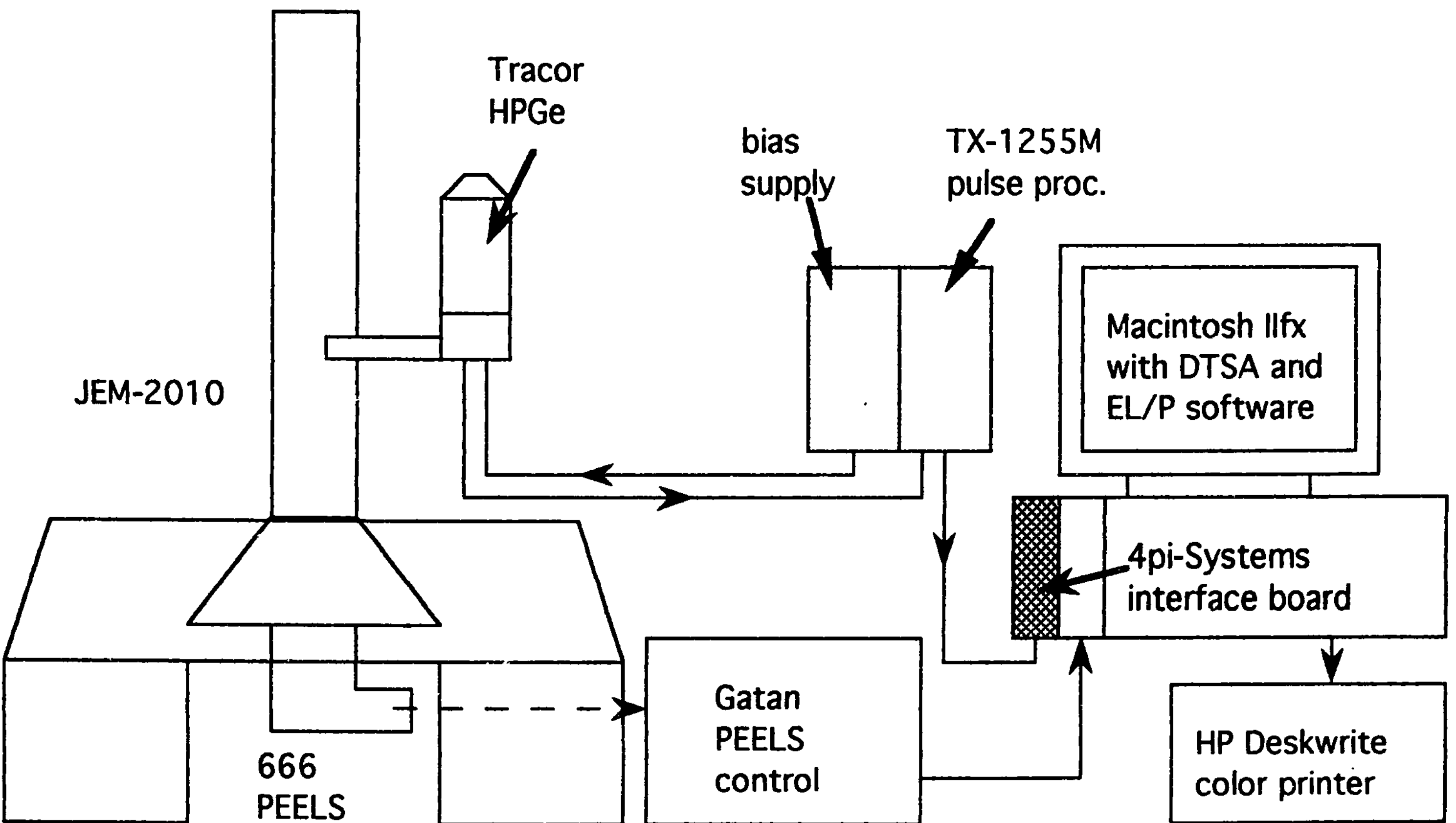

Fig. 5, The AEM system at the Department of Physics, University of Alberta

3.2 EELS system

When fast electrons traverse a thin solid film, they will be scattered by the specimen. The scattering may be elastic or inelastic. The energy-loss spectrum due to inelastic scattering contains information about the specimen composition, structural and electronic properties. The Gatan 666 PEELS system attached to the JEOL-2010 is a parallel-detection electron energy-loss spectrometer (Fig.6). It detects a whole energy loss spectrum simultaneously and is much more efficient than the old style serial instrument.

The spectrometer is mounted at the end of the optical column of the JEOL 2010. The electron beam is bent by a 90° magnetic prism after going through the entrance aperture, which can be set at 1, 2, 3 and 5 mm diameter, the beam is dispersed into an energy spectrum by the magnetic sector. The spectrum is magnified by post-sector quadruple lenses and projected onto the parallel detector. The dispersion settings are 0.05, 0.1, 0.2, 0.3, 0.5, 1.0, and 2.0 eV/ channel. A drift tube voltage can be applied to accelerate the electron beam and thereby provides precise shift of the energy loss spectrum. The energy resolution at zero loss is 1.8 eV when the entrance aperture is set at 3mm. At the carbon K-edge, it is about 2.5 eV. The spectral data is processed by Gatan's EL/P software in the Macintosh IIfx computer.

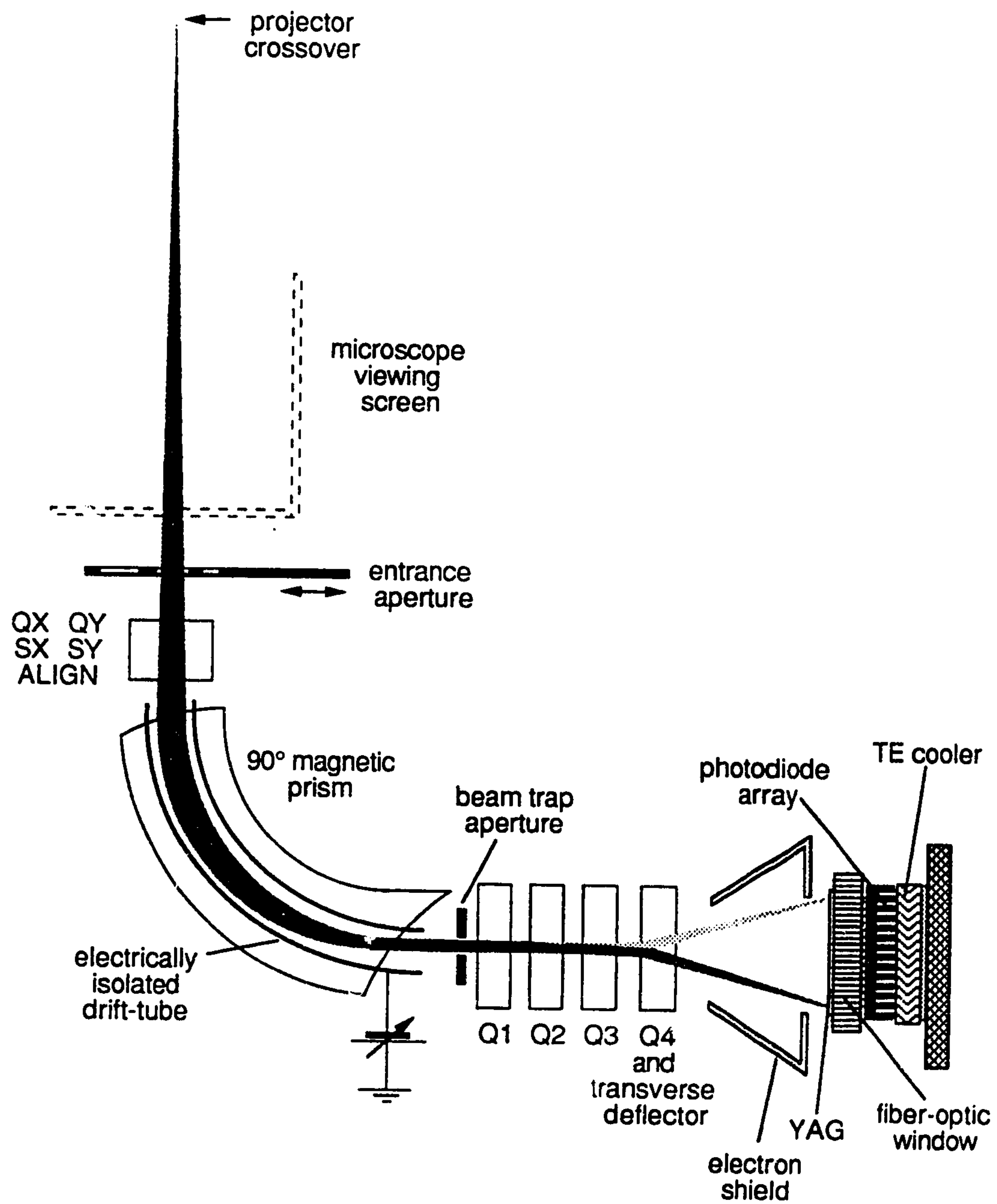

Fig. 6 The Gatan 666 PEELS system

3.2.1 Low loss spectrum and K-shell loss spectrum

Figure 7a and 7b are typical low loss and K-shell loss spectra of CN_x thin films obtained by the Gatan 666 PEELS system when the drift tube voltage was set at 0 and 200V. The low loss spectrum consists of a strong zero loss or elastic peak and a series of plasmon peaks due to plural inelastic scattering from outer-shell electrons. The electron intensity decreases at a high power of energy loss.

There are sharp rises followed by slowly falling intensity, which are assigned to ionization of K-shell electrons. The positions of the sharp edges are approximately the K-shell binding energies of carbon and nitrogen. The shape of the energy loss spectrum reflects the local density of states (LDOS).

By adjusting the beam current and entrance aperture, selecting the proper integrating time and number of readouts in the EL/P software setup menu, we can obtain an energy loss spectrum with very little noise and without saturation. The appearance of the spectrum can be improved by some functions of the EL/P software, like background subtraction and filters.

With the processing and analyzing functions offered by the EL/P software, one can remove plural scattering, sharpen resolution, identify and quantify the edges. In most analysis, the

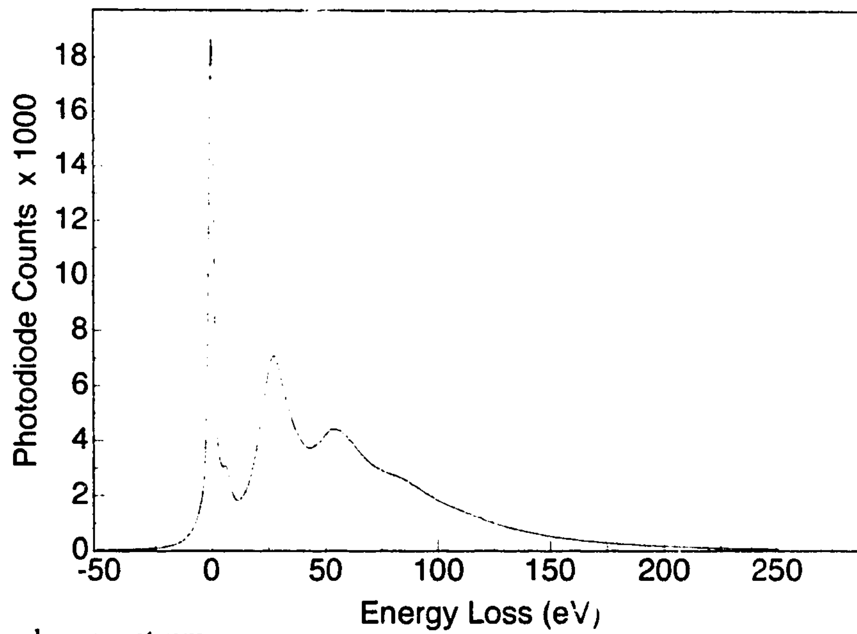

(a) low loss spectrum

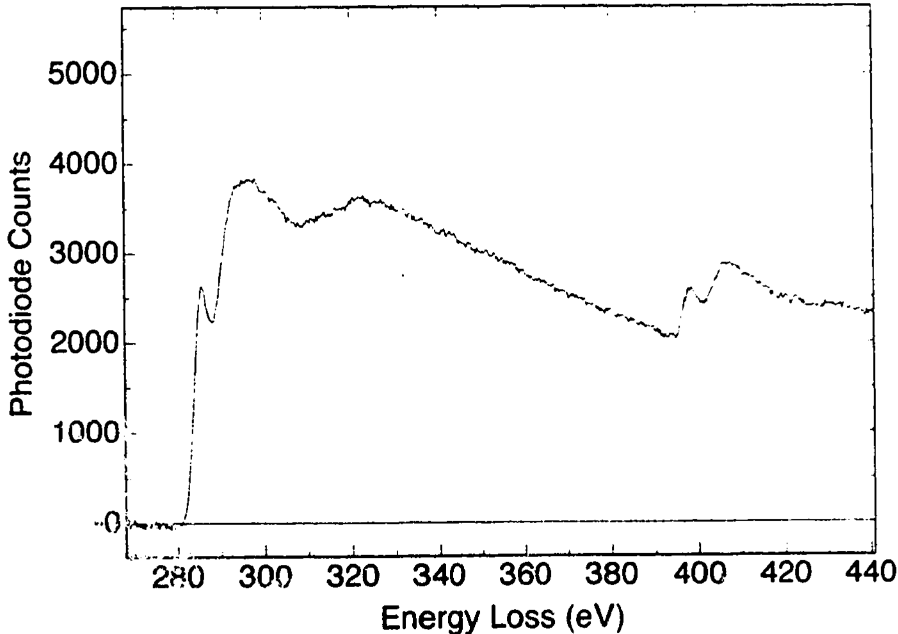

(b) K-shell loss spectrum

Fig 7 Typical EELS of CN_x film

collection angle is a necessary parameter. In order to get the correct value of the angle, we adjust the diffraction focus and brightness knobs to form a focused image of the objective aperture and diffraction pattern on the screen with the TEM in diffraction mode. In this condition, the collection angles (when different objective apertures were inserted) were calibrated and are given in table 2

Table 2 Collection angles for several objective apertures (the manual set)

Objective aperture (μm)	120	60	40	20
Collection angle (mrad)	30	14	11	5.2

3.2.2 Thickness of the films

The thickness t of a thin film can be found from the low loss spectrum in units of λ, the inelastic mean free path (MFP) of electrons (Egerton, 1986).

$$t = \lambda \ln (I_t/I_0) \qquad (3.1)$$

where I_t is the total intensity reaching the spectrometer, I_0 is the zero loss intensity. Because the zero loss peak and the low loss spectrum are overlapped on the energy loss side, the EL/P software assumes a symmetric zero-loss peak and uses the tail on the left side of the peak

to model the tail on the energy-loss side. The integral of counts under this symmetric peak is I_0. Since the intensity decreases at a very high power of energy loss, a 150eV integrate interval is enough for I_t.

The inelastic MFP λ depends on a variety of experimental variables, such as incident electron energy, specimen composition and collection angle.

$$\lambda = 1.66\,(W / \sigma_i \rho)\ \text{cm} \qquad (3.2)$$

where W is the atomic weight, σ_i is the cross section per atom in unit of $cm^2 x 10^{18}$, and ρ is the density of the specimen in unit of $\mu g/cm^3$. When the collection angle β is small enough we can write (Egerton 1986)

$$\sigma_i = (7.5x10^{-24}\ m^2)\ (Z^{1/3} \ln(\beta/\theta_E))\ /\ (\upsilon/c)^2 \qquad (3.3)$$

where Z is the atomic number, υ is the velocity of electrons, $\theta_E = E_m\ (1-\upsilon^2/c^2)/(m_o\upsilon^2)$ is called the characteristic angle corresponding to the mean energy loss E_m. By the above equations, the approximate MFP of the C[illegible]ilms is 120 nm when using the average atomic number and atomic weight of carbon and nitrogen as W. Since we do not know the exact density of the film, the thickness worked out by this way may not be accurate. Fortunately, in the K-shell loss fine structure analysis, we need only the relative thickness in the units of λ. Six locations were randomly selected on each sample in each EELS analysis. The

thicknesses used are the average of the six locations.

3.2.3 Plasmon energy

Each incident electron sets up a plasma oscillation of outer-shell electrons. The energy E_p corresponding to the resonance frequency for plasma oscillation ω_p is called the plasmon energy.

$$E_p = h\omega_p / 2\pi \quad [illegible] \quad m))^{1/2} / (2\pi) \qquad (3.4)$$

where n is the density of electrons and m is the mass of electron. The energy loss function, expressed in terms of plasmon energy E_p and the full width at half-maximum (FWHM) D_{Ep} of the function, is:

$$Im[-1/\varepsilon(E)] = E_p^{\,2} (E\, D_{Ep}) / [(E^2 - E_p^{\,2})^2 + (E\, D_{Ep})^2] \qquad (3.5)$$

We find it reaches a maximum value at an energy loss

$$E_{max} = (E_p^2 - D_{Ep}^2 / 4 + D_E^4 / 128 E_p^2 - \ldots \ldots)^{1/2} \qquad (3.6)$$

By measuring E_{max} in the low loss spectrum to a good approxmation we have

$$E_p = (E_{max}{}^2 + D_{Ep}{}^2 / 4)^{1/2} \quad (3.7)$$

Plasmon energy is a rough measure of thin film density since it is proportional to the square root of electron density. It will change as the film structure changes.

3.2.4 Nitrogen/Carbon ratio of the CNx films

With the energy dispersion at 0.3 eV/channel and the drift tube voltage at 200 V, we can get an energy loss spectrum from 200eV to 500 eV, which covers both carbon and nitrogen K-edges. The areal concentration N (atoms/nm^2) of the atoms giving rise to a ionization edge is (Egerton, 1986)

$$N = (I_e / I) / \sigma \quad (3.8)$$

where I_e is the sum of all counts in that edge over some energy window, I is the sum of all spectrum counts, within an equal energy window, starting at the zero-loss peak, and σ is the cross-section for ionization of an electron in the associated shell. The QUANTIFY EDGE routine in EL/P can automatically identify the edges, compute the partial cross-section, and isolate the edge counts from any background. Without a low loss spectrum, it will calculate the relative areal concentration of the element represented by the

selected edge. Applying this routine to the carbon and nitrogen edges, the N:C ratio x is

$$x = N_{nitrogen}/N_{carbon} \tag{3.9}$$

$N_{nitrogen}$ and N_{carbon} are the areal concentrations of nitrogen and carbon in the film.

3.2.5 Bond structure

By analyzing the fine structure of the EELS spectrum, it is possible to get bond structure information about the specimen.

The hybridization of carbon atoms in compounds could be sp^3 (single bond, 4 σ orbital), sp^2 (double bond, 3 σ orbital and 1 π orbital), and sp (triple bond, 2 σ and 2 π orbital). All the carbon atoms are sp^3 bonded in diamond, and sp^2 bonded in graphite. It is believed that there are sp^2 and sp^3 bonds but no sp bond in various carbon thin films (Robertson 1986). The fraction of sp^3 bonded atoms in a carbon film (which depends on the deposition condition) is dominant in determining its electrical and mechanical properties. This fraction can be obtained from quantitative analysis of both the low loss spectrum and the K-edge fine structure.

The complex dielectric constant $\varepsilon = \varepsilon_1 + i\ \varepsilon_2$ of the film is evaluated by applying

Kramers-Kronig analysis (see program in Fortran in the Appendix) to the low loss spectrum Im $(-\varepsilon^{-1})$. The imaginary part ε_2 represents absorption. A peak in ε_2 at 4 eV is caused by transitions of π electrons, a peak at 13 eV by transitions of σ electrons. The minimum at about 8eV separates π- and σ- electron transitions (fig.8a). By use of a sum rule (Fink et al, 1983) the number of electrons per atom contributing to the optical properties in the frequency range 0 to ω_0 is:

$$n_{eff}(\omega_0) = \frac{m}{2\pi^2 N_a e^2} \int_0^{\omega_0} \omega\, \varepsilon_2(\omega)\, d\omega \qquad (3.10)$$

where N_a is the density of atoms. Taking the sum to 8eV, n_{eff} gives the number of π electrons per carbon atom and integrating up to 40eV gives the number of π+σ electrons. The π to π+σ electron ratio is

$$R_{\pi\sigma} = n_{eff}(8eV) / n_{eff}(40eV) \qquad (3.11)$$

Comparing $R_{\pi\sigma}$ of a sample with that of graphite $R_{\pi\sigma}$(graphite), namely 0.25 (100% of sp^2 bonded atoms), the fractions of sp^2 and sp^3 bonded electrons are

$$R_{sp2} = R_{\pi\sigma} / R_{\pi\sigma}(\text{graphite}) = 4R_{\pi\sigma}, \qquad R_{sp3} = 1 - R_{sp2} \qquad (3.12)$$

The error of this procedure usually is very high (Fink et al estimated a error of about 30%). It mainly comes from the error of Kramers-Kronig analysis near zero loss due to the

arbitrary integration limits, also from the incompletely energy-separated of π- and σ-transitions, corrections for multiple scattering and surface excitation. The poorer the EELS resolution, the worse the Kramers-Kronig analysis results. The FWHM of zero loss peak obtained by the Gatan 666 PEELS system is around 1.8 eV , after Kramers-Kronig analysis, the π peak of ε_2 at 4 eV cannot even be identified (Fig. 8b).

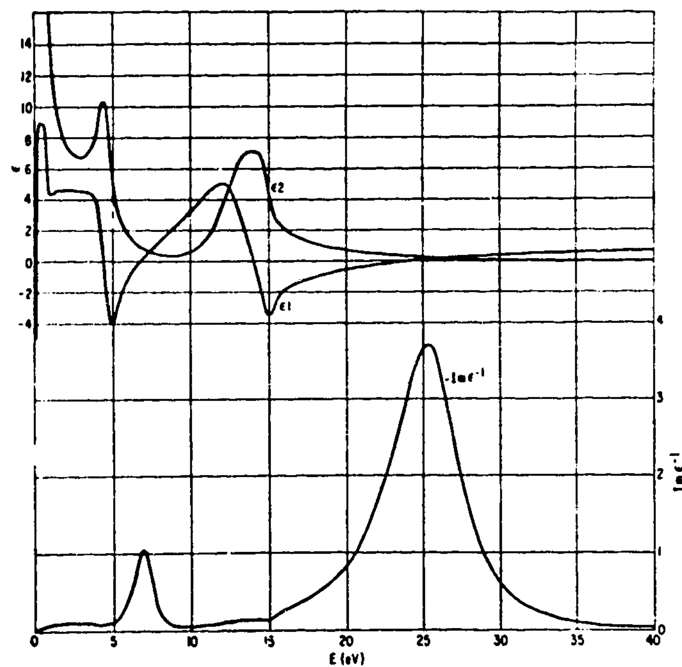

(a) carbon-film data from optical reflection (reproduced from Taft and Philipp, 1965)

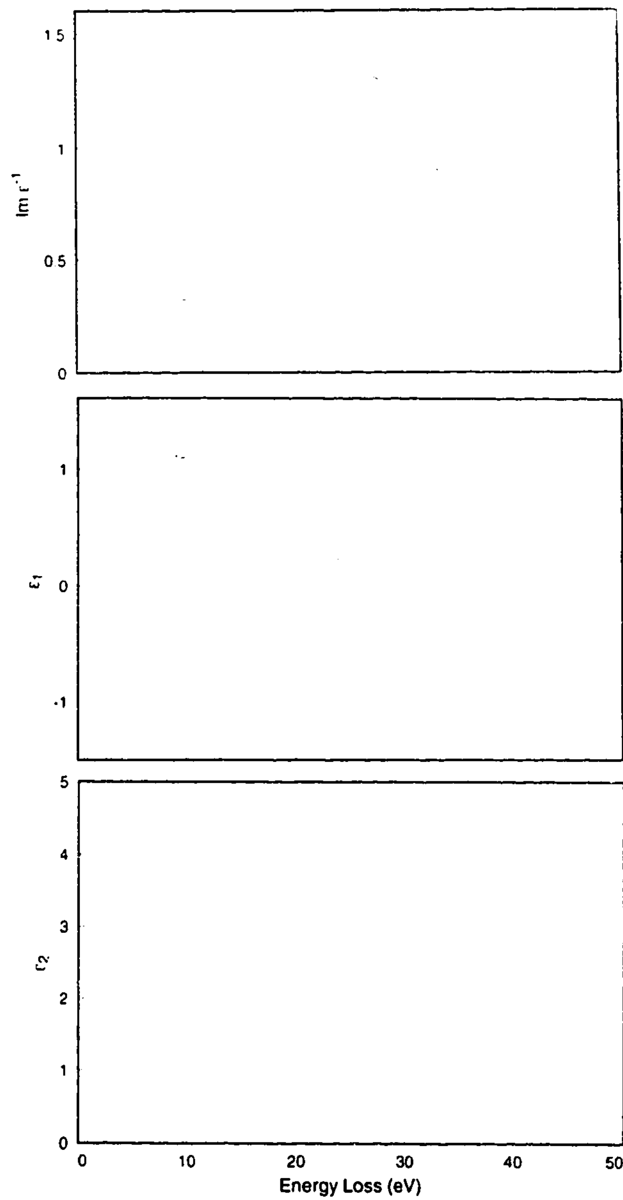

(b) results of our specimen by Gatan 666 PEELS system

Fig. 8 Low loss spectrum of carbon film (after deconvolution) and its dielectric constant

contribution to the π^* peak from σ^* states is small in all forms of carbon (Robertson 1986), the integration of the counts in this peak gives a number which is proportional to the π-bonded electrons in the material. Assuming that the matrix element for the transition from 1s to π^* states is invariant, comparing the integration of π^* peak I_π with that of graphite I_π(graphite), we have

$$R_{sp2} = (I_\pi / I_t) / (I_\pi(\text{graphite})/I_t(\text{graphite})) \qquad (3.13)$$

where I_t and I_t(graphite) are the total integrated counts of specimen and graphite in π^* peak and σ^* peak over some energy window, which are applied to normalize the π^* peaks and make them comparable.

Plural scattering has the effect of reducing intensity in the π^* peak; the loss of intensity increases quickly as the film thickness increases. The EL/P software offers a routine to remove plural scattering by dividing the Fourier transform of the K-shell spectrum by the corresponding Fourier transform of the low loss spectrum, then inverse Fourier transforming. Different thickness causes different loss of the π^* peak intensity, so all the integrations in (3.13) should be obtained after plural scattering removing. Realizing that the observed π^* peak height is proportional to the probability of not exciting a plasmon $\exp(-t/\lambda)$, another way to erase the plural scattering effect is to apply a correction factor $\exp(t/\lambda)$ to I_π and I_π(graphite). The thickness t in the units of λ can be obtained from the corresponding low

way to erase the plural scattering effect is to apply a correction factor $\exp(t/\lambda)$ to I_π and I_π(graphite). The thickness t in the units of λ can be obtained from the corresponding low loss spectrum.

The whole procedure of quantifying the sp^3 bonded electrons includes acquiring a low loss and K-shell loss spectrum of the specimen at the same location, calculating the thickness of the specimen from the low loss spectrum, sharpening the K-shell spectrum with the corresponding zero loss peak, removing the background, fitting the π^* peak with a Lorentz curve directly or after plural scattering removing (Fig. 9), integrating the counts under the Lorentzian and over an energy window to get I_π and I_b and calculating the fraction of sp^2 bonded electron R_{sp2} on the assumption of no sp bond in CN_x films . The energy window we used is 200eV (from 275eV to 475 eV).

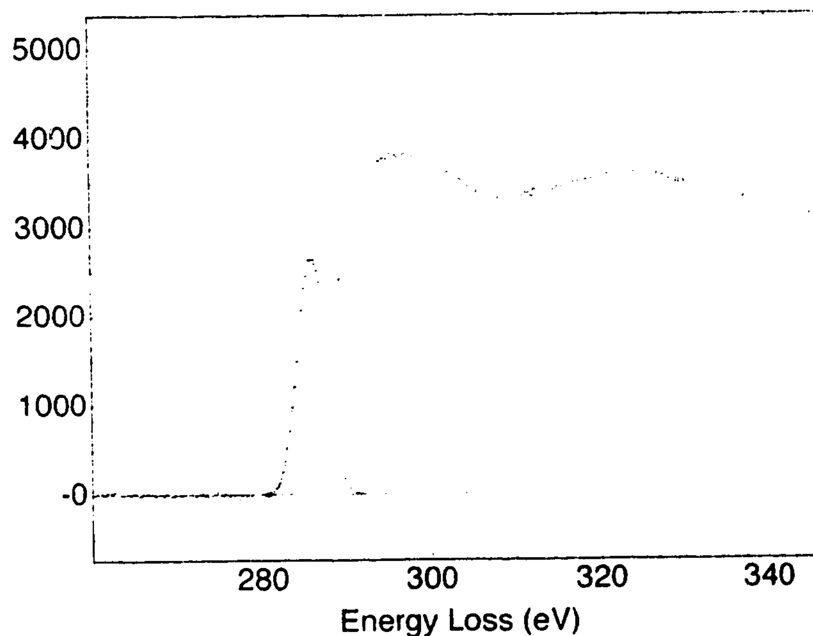

Fig. 9 Fit of the π^* peak with a Lorentzian

angle (Egerton, 1986), so crystalline graphite can not serve as a standard. Fortunately, arc-discharge evaporated amorphous carbon film will totally graphitize when heated to above 500°C, and the electrons in amorphous carbon films d.c.-sputtered in Ar ambient at room temperature are also 100% sp^2 bonded (Fink et al. 1983). They can serve as standards.

Another way to obtain the fraction of sp^2 or sp^3 bonds from EELS was suggested by Wang et al. (1990). From the differential low loss energy spectrum, π and $\pi+\sigma$ plasmon energies $E_p(\pi)$ and $E_p(\pi+\sigma)$ were located. From Drude model we know the square of these plasmon energies are proportional to the effective concentration of electrons participating in the plasma resonance C. For π plasmon, C_π is proportional to R_{sp2}; for $\pi+\sigma$ plasmon, $C_{\pi+\sigma}$ is proportional to $R_{sp3}+R_{sp2}$. Then we have (see Wang et al. for details):

$$R_{sp2} = 4\, E_p(\pi)^2 / 0.23\, E_p(\pi+\sigma)^2 \qquad (3.14)$$

Similar to the sum rule method, this method works only when the EELS resolution is high enough.

3.3 Energy-Dispersive X-ray spectrometer (EDX)

The de-excitation of excited or ionized atom by fast electrons involves emission of Auger electrons and characteristic x-ray. The x-rays have a photon energy equal to the difference in binding energy of the initial and final states of the electron which fills the vacant core level. They are specific to the atomic number and inner-shell of the emitting atom, hence permit elemental analysis.

Emitted x-rays can be detected by a reverse-biassed silicon or germanium diode cooled with liquid nitrogen. Each x-ray photon creates a current pulse whose height is proportional to photon energy. A pulse-height analysis circuit counts and analyses the pulses, and gives a plot of the number of photons against photon energy . Figure 10 is a typical EDX spectrum of a CN_x film .

The x-ray emission spectrometry system fitted to the JEOL 2010 TEM consists of a Noran high-purity germanium detector with low Z window; a Noran nuclear instrument module (NIM) works as power supply, amplifier, and pulse processor. Spectra data is accumulated and processed by the Macintosh IIfx computer, under the control of "DTSA" software.

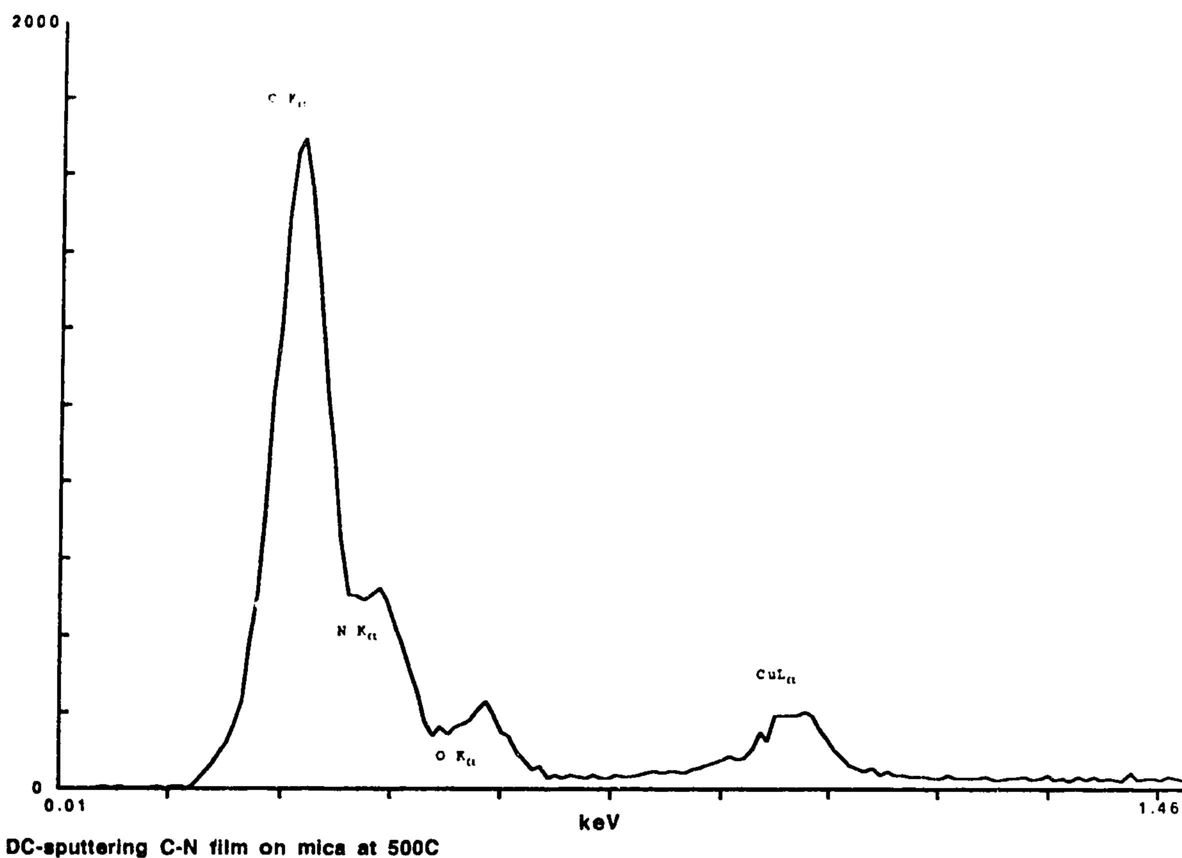

Fig. 10 EDX spectrum of CN_x thin film (by sputtering, x=0.4)

The germanium detector with low Z window is able to detect all elements down to beryllium. The relative elemental concentration is given by

$$C = k_{ab}(I_a/I_b) \tag{3.12}$$

where I_a and I_b are integrations of counts under K-peaks of element a and b. k_{ab} is the correction factor (k factor) of element a over b. There are many sources which affect the k

electron energy and intensity due to inelastic scattering. Usually k_{ab} is obtained by experiment , measuring the k factor of a standard sample which contains both elements a and b with known composition, or of two samples both contains one element of a or b and a reference element c, then

$$k_{ab} = k_{ac} / k_{bc} \quad . \qquad (3.13)$$

Chapter 4 RESULTS AND DISCUSSIONS

27 CN_x films (8 by evaporation, 19 by sputtering) were deposited to a thickness of less than 100nm and analyzed by the AEM system. TEM bright-field images show that most as-deposited CN_x films are uniform (Fig. 11a). The diffuse rings in their diffraction patterns (Fig. 11b) reveal that they are predominantly amorphous with a small fraction of nanometer sized crystallites.

When exposured to an electron beam, the films deposited on a substrate at room temperature without annealing will be easily damaged by electrostatic charging, which indicates high resistivity of the films. An area for examination must be selected around a grid corner to avoid such damage. The resistivity of those films, roughly measured with a Keithley 615 digital electrometer, is about 10^8 Ω-cm, which is higher than that of vacuum arc evaporated carbon film (10^4 Ω-cm) but lower than that of carbon film deposited in Ar ambient at the same pressure (>10^9 Ω-cm). It turns out that the increase of resistivity is mainly contributed by the pores and voids in the films, and increased nitrogen concentration will improve the conductivity. After annealing, the resistivity is 2 orders lower.

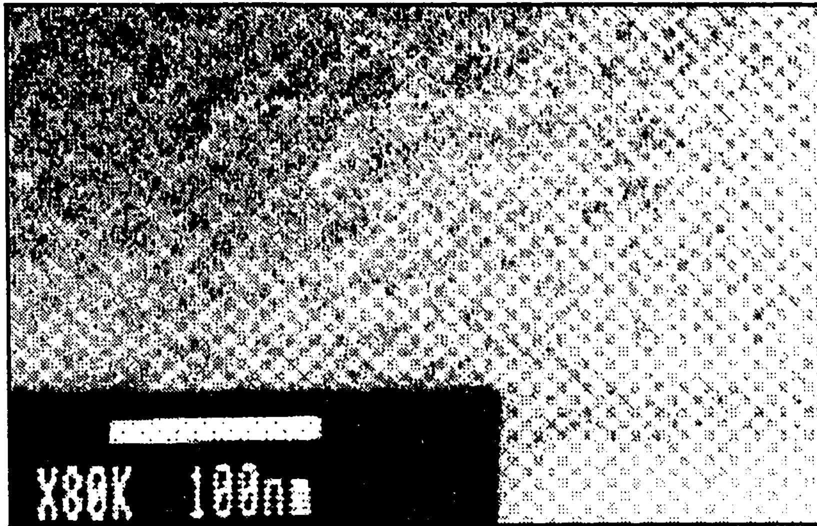

(a)

TEM image

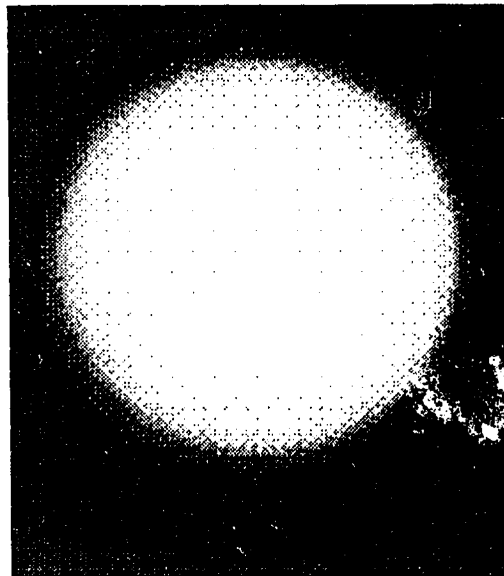

(b) Diffraction pattern

Fig. 11 TEM image and diffraction pattern of a CN_x film deposited by DC-sputtering in 20 mTorr N_2, at 40 watts power on KCl substrate

4.1 Nitrogen/carbon ratio

The nitrogen/carbon concentration ratio x of CN_x thin films depends on deposition conditions and later treatments. Th[illegible] no nitrogen detected by either EDX or EELS in the specimen made by arc-discharge evaporation in nitrogen ambient without a bias on the substrate, but some nitrogen in the sample deposited in ammonia (Table 3). When bias is applied to the substrate, whether positive or negative, the nitrogen concentration increases significantly (in both nitrogen and ammonia ambient). By sputtering at room temperature, x could be as high as 0.57. All the data in table 3 are from EELS.

In nitrogen gas, the nitrogen atoms are strongly bonded in the form of N_2 molecules. The ionization potential of 15.6 eV is much higher than the average energy of carbon particles and electrons generated by an arc-discharge. There is little chance for N_2 to be broken into atoms or ions and incorporated into the carbon. The ionization ($NH_3 \rightarrow N^{3-} + 3H^{+}$) potential of ammonia is lower (10.2eV); moreover the three N-H bonds could be broken one by one, which makes NH_3 a better ambient than N_2. The bias applied to the substrate increases the particles energy up to 50 eV, which assists the ionization of nitrogen. The higher nitrogen concentration with positive bias (Table 3) results from the higher electron energy which gives more nitrogen ions in the ambient; it also results from the lower carbon particles energy which gives less dissociation of C-N bonds in the CN_x film due to resputtering.

During sputtering, most of the nitrogen in the plasma is in the form of ions. The nitrogen content is limited by dissociation of C-N bonds.

Table 3 N/C ratio x of CN_x thin films deposited at different conditions before and after annealing to 800°C

Deposition condition	sputtering	arc(zero bias)	arc(+ bias)		arc(- bias)	
Working gas	NH_3	NH_3	N_2	NH_3	N_2	NH_3
x Before anneal	0.48	0.09	0.10	0.25	0.14	0.19
x After anneal	0.07	0.08	0.04	0.08	0.06	0.08

4.1.1 The effect of electron beam irradiation

When a specimen is studied in a TEM, it is exposed to a high energy (200 keV) electron beam. The excitation caused by high energy electrons could change the structure and composition of the specimen. Figure 12 is the change of N/C ratio of a d.c sputtered CN_x film under electron beam irradiation for more than 30 minutes. The EDX and EELS spectra were collected from a fixed location of the sample every 10 -15 minutes. The result from EDX (Fig. 12a) shows a 20% random change which we assign to statistical error. The k-factor is obtained by comparing the result with EELS: k_{CN} is equal to 0.88. EELS gives a

more accurate result (Fig. 12b). The nitrogen loss in 56 minutes is less than 5%.

Since no change of thickness and EELS carbon and nitrogen K-shell fine structure was observed, it can be concluded that the C-N bond is fairly stable against high energy electron beam irradiation.

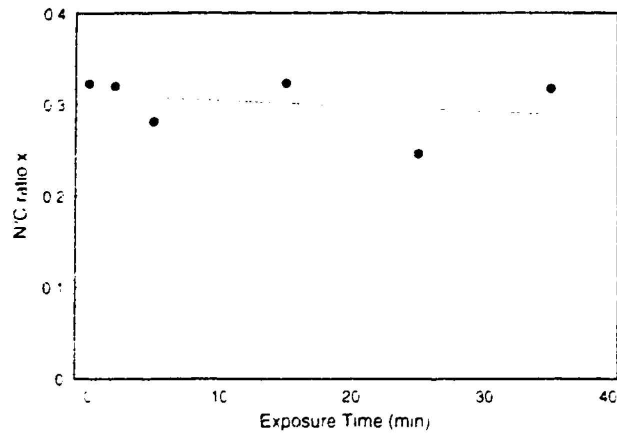

(a) by EDX

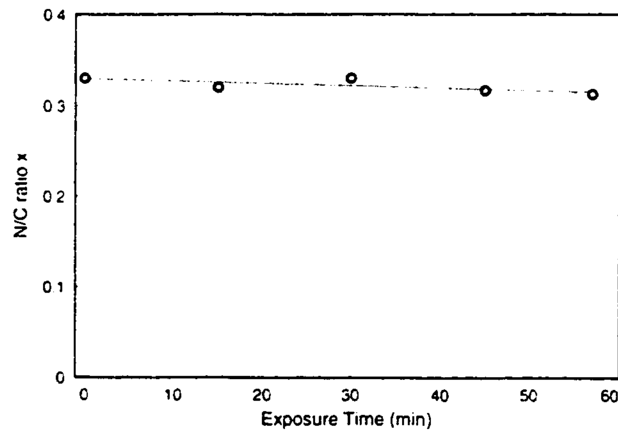

(b) by EELS

Fig. 12 The change of N/C ratio of an DC sputtered CNx thin film under electron beam irradiation

4.1.2 Effect of annealing

Some of the samples were transferred to the vacuum chamber to be annealed. The vacuum system is the one used for carbon arc discharge evaporation. A tungsten evaporation boat was used as a heater. The CN_x filmson TEM grids were directly loaded into the boat The annealing was carried out at 7×10^{-6} torr. The temperature was measured by a thermocouple attached to the boat.

EELS analysis of these annealed films showed that there was little change of N/C ratio after the films were annealed to 300°C. However above 600°C nitrogen concentration decreased sharply. The N/C ratios of CN_x films deposited at different conditions after annealing to 800°C are listed in table 3 (page 43).

After annealing to 800°C more than 75% of the nitrogen was lost, but a small fraction of nitrogen (<25%) was left even after annealing at above 1000°C. The final N/C ratio is about 0.07. The behavior agrees with the recent reports of Freire et al (1994) and Mariotto et al (1994). It suggests that there are at least two different C-N bonds in the film. One is weaker than the graphite C-C bond with an energy of the order of $k_B T = 0.1$ eV. The other is stronger and stable.

4.1.3 Effect of substrate temperature

Substrate temperature can be controlled during sputtering. The N/C ratio x decreases almost linearly as the temperature rises (fig. 13). It agrees with the analysis of annealing results, in which the high substrate temperature caused the weak C-N bonds' dissociation. Since the N/C ratio of the CN_x film deposited at 600°C is much higher than that of the film deposited at room temperature but annealed to 600°C, we can conclude that higher substrate temperature is helpful in forming the strong C-N bond. Although the highest x we obtained by sputtering on a cooled substrate reached 0.75, which is higher than any other reported

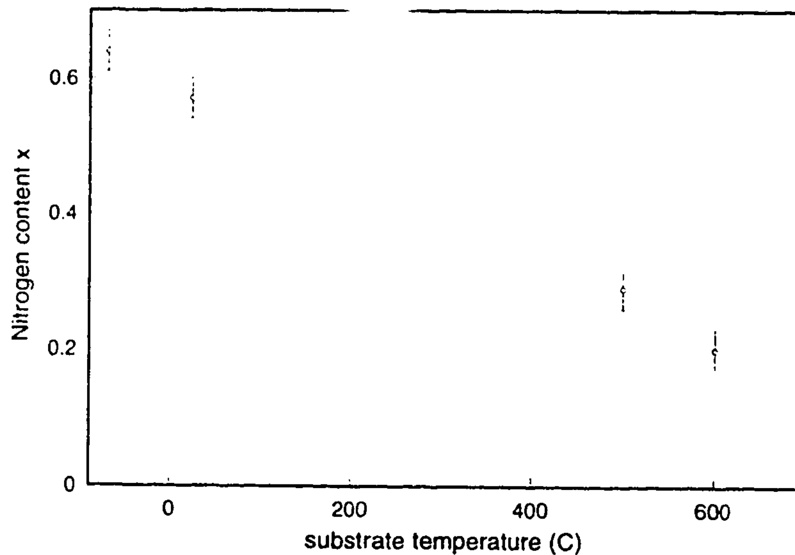

Fig. 13 N/C ratio x depends on substrate temperature (Deposition condition: d.c. sputtering in 20 mTorr N_2, at 40 watt power on mica substrate)

sputtering results, it is still far from that of β-C_3N_4, namely 1.33. Furthermore, the stability of the as-deposited CN_x films is much poorer than that of the predicted β-C_3N_4.

An interesting phenomenon was found when a CN_x film was deposited on heated KCl substrate: the CN_x formed a replica of the evaporated KCl surface (fig 14), which may help us to understand the crystallization of KCl.

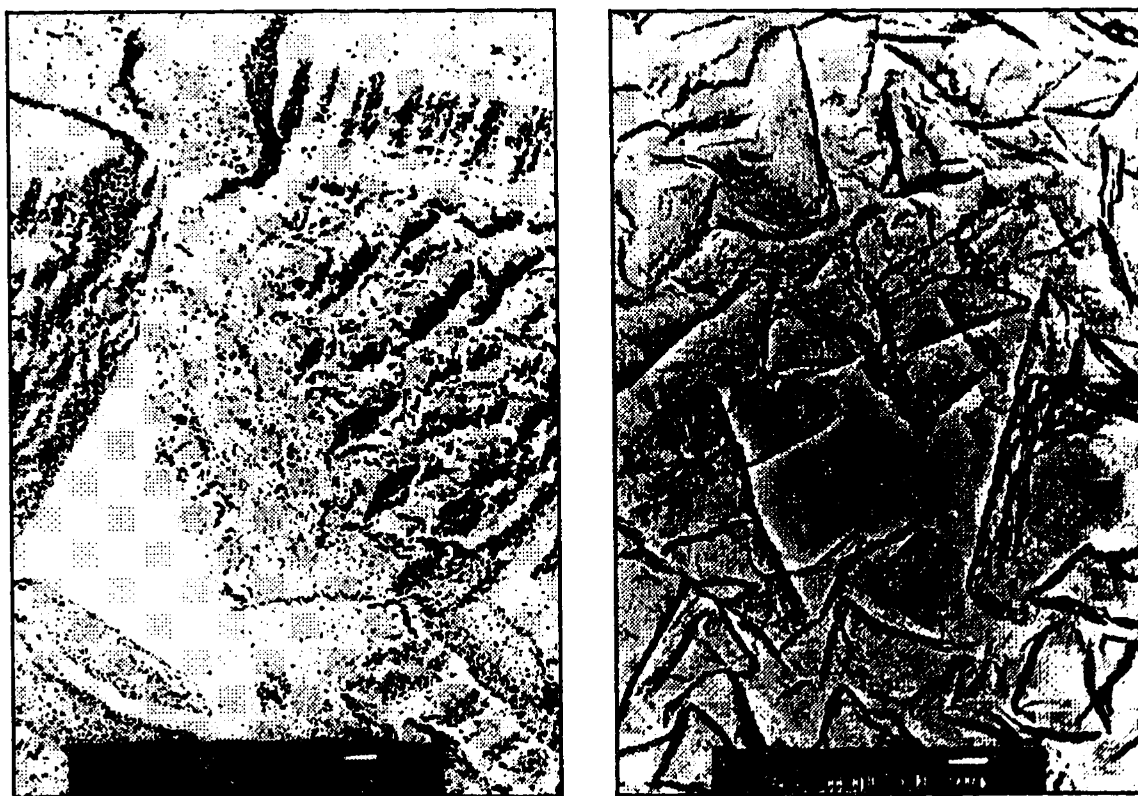

Fig. 14 CN_x replica of evaporated KCl surface

4.1.4 Effect of other sputtering parameters

The N/C ratio x depends on many other sputtering parameters such as power, pressure, working gases and substrate. Some examples are given in table 4. It seems that the substrate has little effect on N/C ratio but that higher sputtering energy and higher nitrogen pressure have a negative effect on the incorporation of carbon and nitrogen.

Table 4 Dependence of N/C ratio x on sputtering conditions

a	Pressure	20 mTorr	100 mTorr	
	x	0.20	0.04	
	R_{sp2}	1.13	0.81	
b	Power	40 W	300 W	
	x	0.29	0.20	
	R_{sp2}	1.21	1.14	
c	Working gas	N_2	Ar/N_2	
	x	0.29	0.16	
	R_{sp2}	1.21	1.10	
d	Substrate	KCl	mica	silicon
	x	0.29	0.29	0.29
	R_{sp2}	1.21	0.98	1.13

4.2 Bond Structure

By K-shell loss fine structure analysis, the intensity ratio of π^* peak to $\pi^* + \sigma^*$ peak of an amorphous carbon film deposited by vacuum arc-discharge is $(3.2 \pm 0.1) \times 10^{-2}$. After annealing it is $(3.5 \pm 0.2) \times 10^{-2}$. Assuming that the annealed film is 100% sp^2 bonded, then the original film is 92% sp^2 bonded. This result agrees with previous work of other groups (Berger, McKenzie, Martin, 1988, Fink et al, 1983), and confirmed that the method is applicable to pure carbon films.

Table 5 Comparison of two plural scattering removed methods

Sample	1	2	3	4	5	6	7
R_{sp2} (Method1)	1.94	1.75	1.70	1.32	1.12	1.13	0.94
R_{sp2} (Method2)	1.94	1.68	1.70	1.37	1.18	1.04	0.95

Table 5 gives the fractions of sp^2 bonded electrons of seven CN_x samples by two different methods for removing plural scattering. Method 1 uses a thickness factor (page 35), Method 2 is by deconvolution (page 34). The two methods match well. The largest discrepancy between the two methods is less than 10%. Essentially the two methods are same but by

removing the plural scattering by deconvolution, we can directly compare the energy loss spectra and usually need a relatively smaller integration window.

In most CN_x samples, the fractions of sp^2 bonded electrons obtained by K-shell fine structure analysis exceed 100%, which suggests that something is wrong in our application of the method to CN_x thin films. One possibility is that the assumption of no sp-bonded electrons in CN_x film may not be true. From the previous analysis, we know that the ratio of π bonded electrons to σ bonded electrons of different carbon hybridizations are 0:4 (sp^3), 1:3 (sp^2), and 2:2 (sp). If we use the ratio of counts in π peak to total counts to scale the fraction of sp^2 bonded electrons, and set this ratio of graphite as 1 (R_{sp2} in equation 3.11), then the R_{sp2} value of a 100% sp bonded sample will be 200%. Generally a film which contains sp, sp^2, and sp^3 bonds has a R_{sp2} value between 0 to 200%, which covers all the experiment results we got (54% to 195%). The R_{sp2} values exceeding 100% suggest the existence of sp bonding. Fourier transform infrared spectrum (FT-IR) results on CN_x film by different groups (Cuomo et al., 1979, Han and Feldman 1988, Nakayama et al, 1993, Ogata et al. 1994) showed an absorption peak near 2200 cm^{-1}. Its intensity increased as nitrogen content increased. An isotope shift of 31 cm^{-1} of this peak was found when ^{15}N was substituted for ^{14}N (Kaufman et al. 1989). This shift was believed to be proof that the 2200 cm^{-1} peak could be assigned to the C≡N bond (Pinchas and Laulicht, 1971). Another absorption peak at 1600 cm^{-1} in FT-IR of CN_x films was assigned to the C=N bond.

X-ray photoelectron spectroscopy (XPS) results from other workers showed that there are

three to four binding energies of carbon and nitrogen which are different from the binding energies of C-C, N-N, C-O and N-O in CN_x films deposited by sputtering, ECR, and IBD.(Hoffman et al, 1993, Fujimoto and Ogata, 1990, Bousetta et al, 1994, Marton et al, 1994). This suggests that carbon and nitrogen can be combined in different bonds. By comparing the XPS of pure graphite and polyacrylonitrile fibers, Rossi et al. (1994) attributed the two peaks at 398.2eV and 400.2eV to C≡N and C=N. Their IR results (absorption peak at 1220cm^{-1}) also suggested the existence of C-N single bonds. Torng et al. (1990) concluded from the shift of carbon 1s binding energy and the change of fine structure of XPS that there are more sp^3 bonded electrons in CN_x film than in pure carbon film. On the other hand, optical absorption and dc electrical conductivity measurements revealed that sp^3 bonds were destroyed by the nitrogen incorporation (Doll, et al, 1993). All the evidence tells us that CN_x is a complicated system; its properties may be totally different depending on the deposition conditions.

Another possible reason for R_{sp2} of CN_x thin films exceeding 100% could be charge transfer between carbon and nitrogen atoms. The outer-shell π electrons of carbon atoms will transfer to a neighboring nitrogen atom, since the electronegativity of nitrogen is higher (N: 3.0, C: 2.5). Emptying the carbon π band will lead to extra intensity in π^* peak, because π and π^* bands of graphite are overlapped (Cox, 1987), which results in an abnormal R_{sp2} value. On the other hand, the π^* peak of nitrogen will be reduced. The more nitrogen is incorporated, the higher the carbon π^* peak, and the lower the nitrogen π^* peak. Figure 15 is the comparison of carbon and nitrogen K-shell loss fine structure, the carbon K-edge was shifted

to 400 eV to match that of nitrogen. When the N/C ratio x is 0.1 (fig. 15a), the carbon π^* peak is less prominent than the nitrogen π^* peak; when x increases to 0.4 (fig. 15b), their intensities are almost identical. When x equal to 0.6 (fig. 15c), we can see clearly that the nitrogen π^* peak is reduced while the carbon π^* peak has increased. That the ratios I_π/I_σ of carbon and nitrogen change in the opposite direction could be evidence of charge transfer. On the other hand, the different fine structure of carbon K-edge and nitrogen K-edge might suggest that in CN_x films, there are more carbon-carbon triple bonds and more carbon-nitrogen single bonds as nitrogen content increases. This ambiguity in interpretation points to a limitation of EELS for quantifying the bond structure of CN_x films.

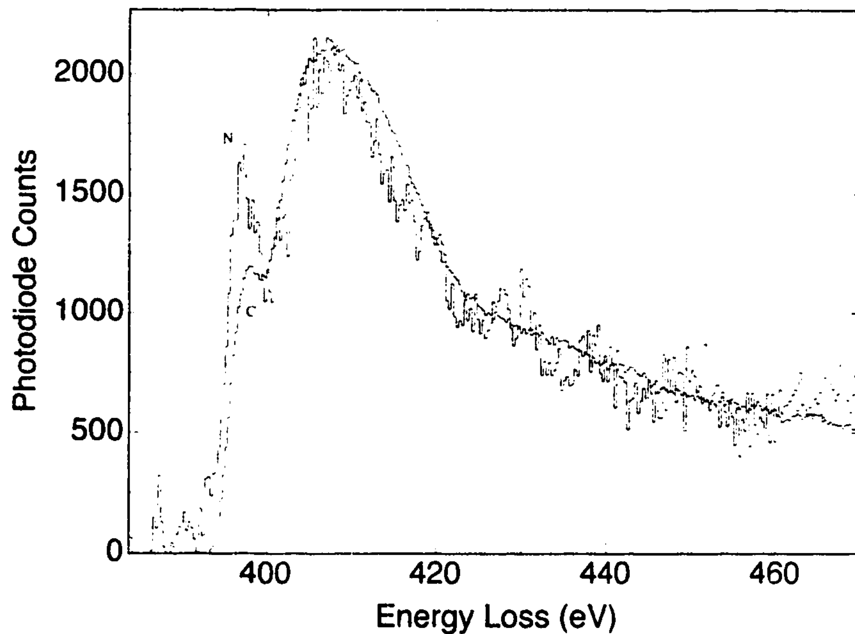

(a) N/C ratio = 0.1

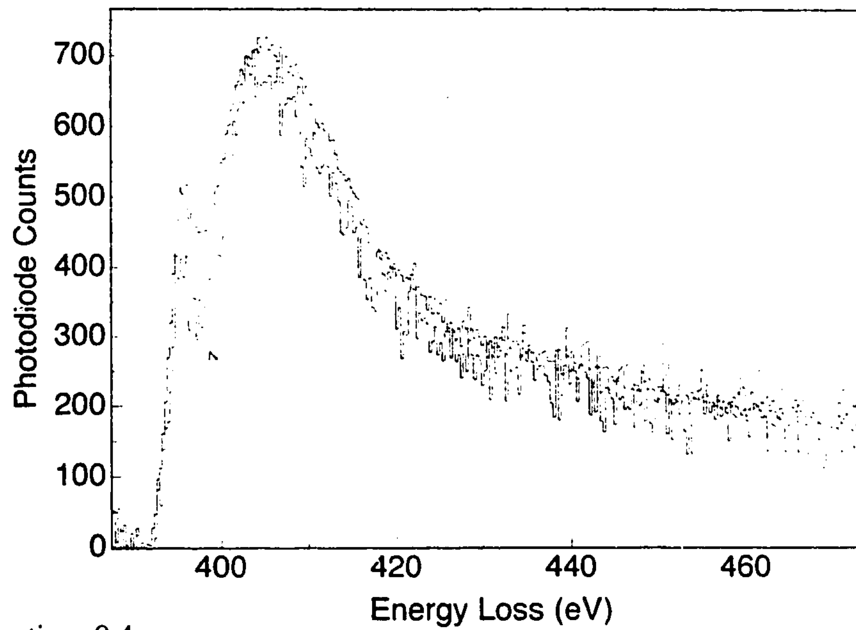

(b) N/C ratio = 0.4

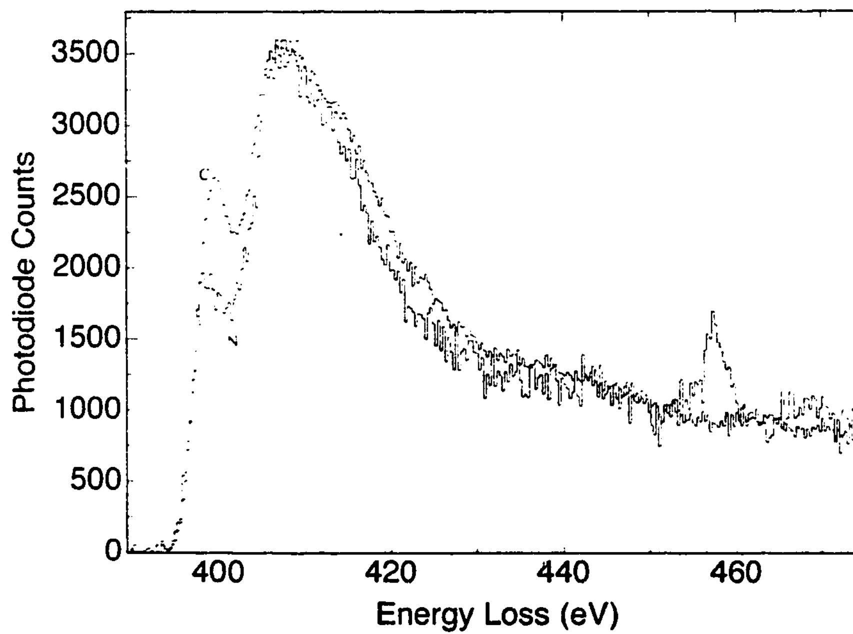

(c) N/C ratio = 0.6

Fig. 15 comparison of carbon and nitrogen K-shell loss fine structure.

4.2.1 The dependence of R_{sp2} on N/C ratio x and substrate temperature

The spectra shown in the previous section gave an example of how R_{sp2} increases as the N/C ratio x increases. Figure 16 gives a more general dependence of R_{sp2} on x. The error bars are from the results at six different locations. In most cases, R_{sp2} is greater than 100%, and tends to increase as nitrogen concentration increases, although it varies a little with deposition conditions. This result supports the theory of π-electron transfer since higher nitrogen content should increase the overall amount of transfer. However, it is also possible that nitrogen is favorable for carbon sp hybridization.

A few cases where $R_{sp2} < 100\%$ occur in the case of CN_x films deposited at high substrate temperatures . This supports the conclusion from chapter 4.1 that high substrate temperature helps the formation of strong sp^3 bonds. Figure 17 shows the dependence of R_{sp2} on substrate temperature. As temperature rises, R_{sp2} decreases probably due to the loss of nitrogen. The fractional decrease in R_{sp2} and N/C ratio x are of the same order.

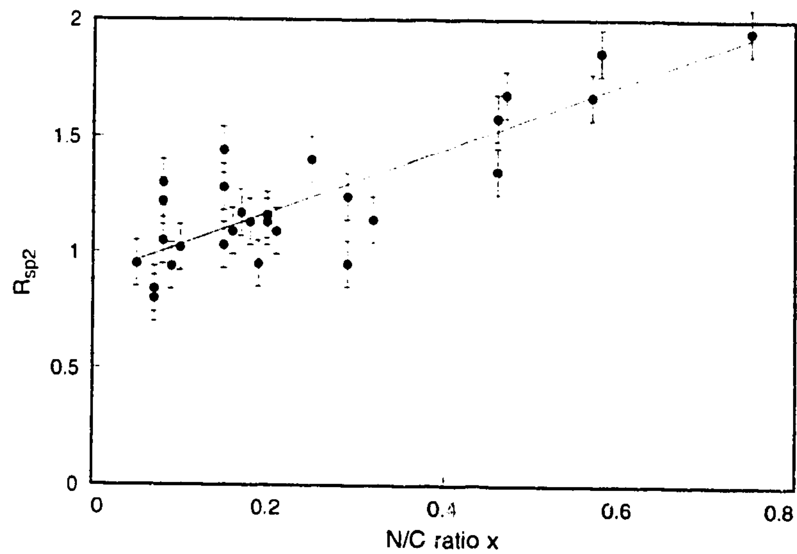

Fig. 16 Dependence of R_{sp2} on N/C ratio x

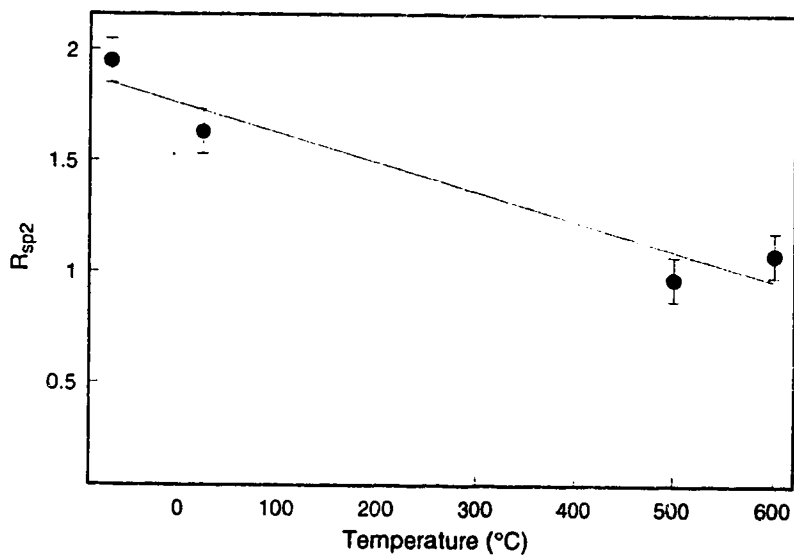

Fig 17 Dependence of R_{sp2} on substrate temperature

4.2.2 Effect of annealing

After annealing, R_{sp2} changes in two different ways as nitrogen is lost (Fig. 18) : increasing in those arc-evaporated films with negative bias (the third and fourth data points in fig. 18), but decreasing in all other films . There are two processes in the CN_x films caused by annealing: dissociation of C-N bonds which decreases the R_{sp2} value, and graphitizing of amorphous carbon which increases the R_{sp2} value. Comparing with films of the same nitrogen content, the original R_{sp2} value of negative bias arc-evaporated films is relatively low. The low original R_{sp2} and the increasing of R_{sp2} by annealing indicate the C-N bonds or C-C bonds in those films are more sp^3 like, which suggests that carbon-ion bombardment during deposition assists the forming of sp^3 bonds.

After annealing, the K-shell π peak of nitrogen is much smaller than that of the film not annealed but originally with low nitrogen content (x=0.8), although their carbon π peaks were very similar. Clearly the C-N bonds in these two films are different.

4.2.3 Dependence of R_{sp2} on other sputtering parameters

Table 4 listed some examples difference in R_{sp2} due to the changes of pressure, sputtering power, working gas and substrate type. It is hard to evaluate their relationship since N/C

ratio x changed simultaneously. But obviously mica is a much better substrate than KCl in terms of lower π peak. The R_{sp2} value of the film deposited on it is 23% lower than that of film deposited on KCl with the same nitrogen content.

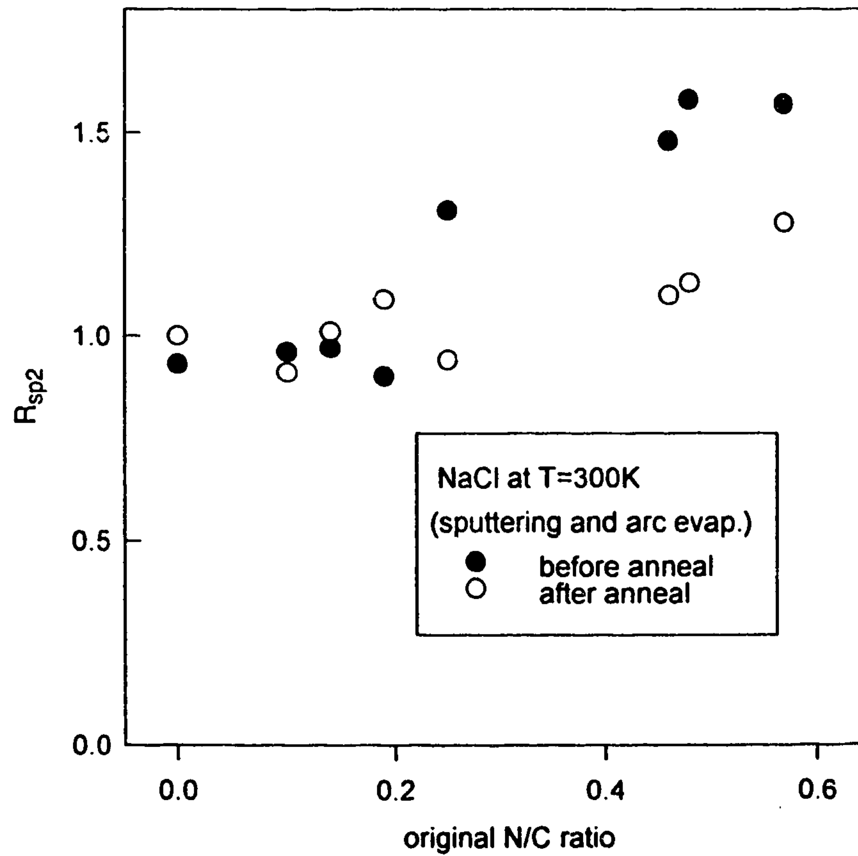

Fig. 18 Effect of annealing on R_{sp2}

4.3 Plasmon energy

It was found by Fallon and Brown (1993) that the plasmon energy of amorphous carbon films increases linearly with the percentage of sp^3 bonding (Fig. 19a). Their data can be fitted onto a straight line which ranges from graphitized carbon film through diamond. However some forms of carbon such as graphite and the fullerenes show a higher densityof electrons, while hydrogen-containing carbon shows a lower one. This is easy to understand because the plasmon energy is proportional to the square root of density which is determined by bond structure. From the analysis in Chapter 3 (3.14), we have:

$$R_{sp3} = 1 - 4\, E_p(\pi)^2 / 0.23\, E_p(\pi+\sigma)^2 \qquad (4.1)$$

where $E_p(\pi+\sigma)$ is the plasmon energy we are discussing. Considering a small interval of $E_p(\pi+\sigma)$, for example 20eV - 30eV, (4.1) tells us R_{sp3} increases linearly with plasmon energy. Figure 19b shows the relationship between R_{sp2} values obtained by K-shell fine structure analysis and their plasmon energies. The plasmon energies vary randomly between 24eV to 27eV but the difference of R_{sp2} values is as high as 100%. Once more, the fact that R_{sp2} does not relate directly to the bond structure of CN_x films is proven.

Generally, the plasmon energy of a CN_x film is about 2-3eV lower than that of vacuum

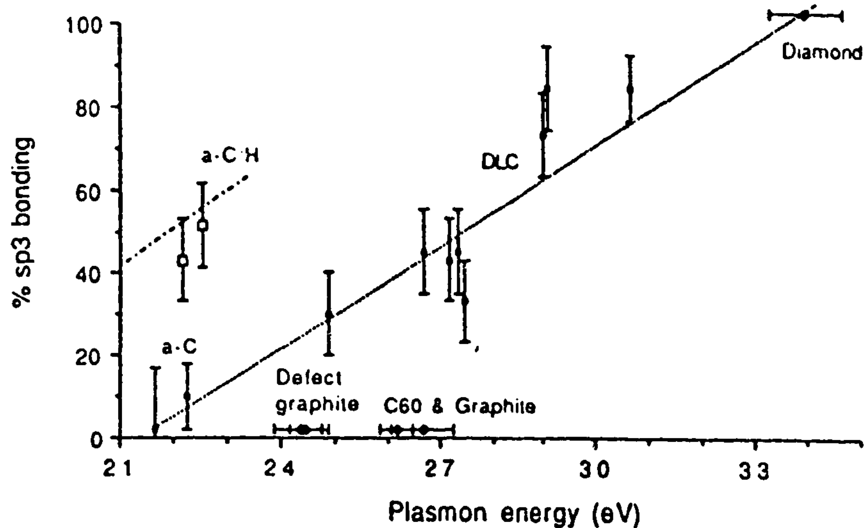

(a) carbon films (reproduced from Fallon and Brown, 1993)

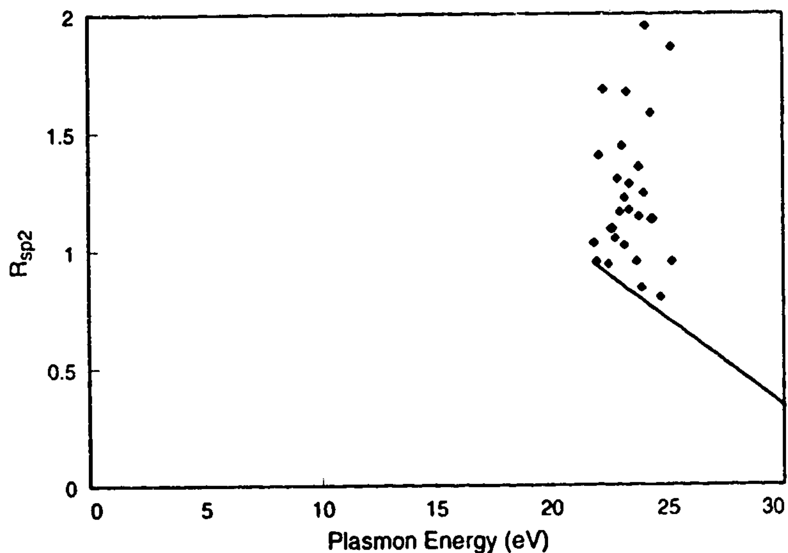

(b) CN_x films, the straight line is corresponding to the dotted line in (a)

Fig. 19 Relationship of R_{sp3}/R_{sp2} and plasmon energy

arc-evaporated amorphous carbon film, which could be the result of more voids and pores in a film deposited in a poor vacuum. The plasmon energy changes very little when deposition conditions change, even after a high-temperature anneal. Only when the substrate temperature is very high or very low does the plasmon energy increase.

4.4 The Occurrence of Crystallites

We did not find any evidence of β-C_3N_4 crystallites in our films, but we did find some crystalline areas in the CN_x films deposited by sputtering onto a silicon {100} substrate at 500°C. The crystallites are about 100nm in diameter, randomly distributed in the film and occupying about 10% of the film area (Fig. 20a), which is very similar to the description of the Berkeley group (Yu et al. 1994) who claimed what they found is β-C_3N_4. The deposition conditions are almost the same except they used RF-sputtering while we used DC-sputtering and deposition on mica, KCl and silicon. Figure 20b is the selected area diffraction pattern of the crystallite. The d-spacings are listed in table 6 , together with those of the predicted β-C_3N_4, silicon, and graphite. The predicted β-C_3N_4 values are calculated by the Macintosh software package DIFFRACT. There are more cases of mismatch than of matching between the TED results for this crystalline material and the predicted β-C_3N_4 values.

On average, the energy-loss spectrum of the CN_x film containing crystallites is close to that

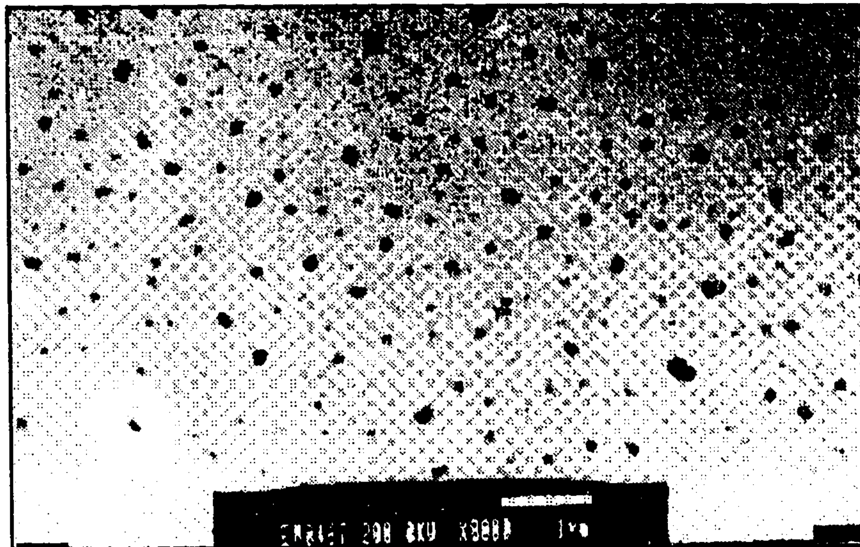

(a) TEM image

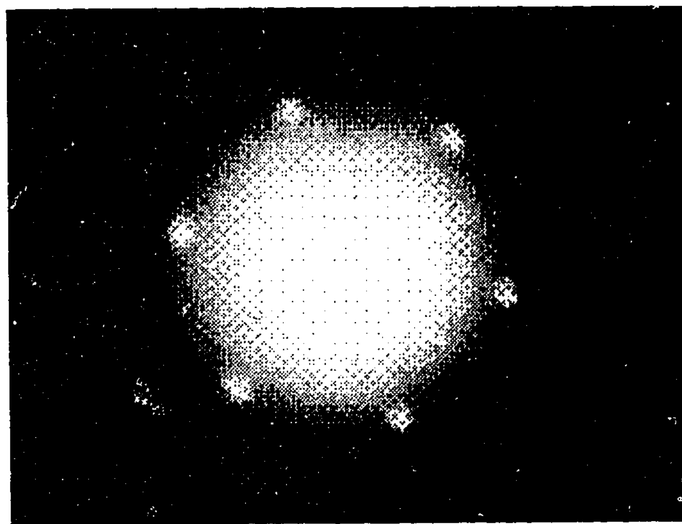

(b) Diffraction pattern

Fig. 20 TEM image and diffraction pattern of a CN_x film containing crystallites

of other films. The micro-probe results on the crystallite show something different. The selected area EELS is given in Figure 21. The plasmon energy of the crystallite is 30 eV, much higher than in the amorphous area. The π^* peak intensity is much lower; R_{sp2} is only 0.84; The N/C ratio is about 13% lower than in the amorphous area. But the EELS K-edge looks like a potassium L-edge superposed on the carbon K-edge. The EDX spectrum of the crystallites shows a strong peak of potassium, which was not found in the amorphous area. The potassium may come from the evaporation of the KCl substrate. This crystalline material became amorphous rapidly under electron beam irradiation. The diffraction spot disappeared in a couple of minutes. In later deposition on a single silicon substrate, no such crystalline regions were found. The crystallites could be the product of two processes: reactive sputtering in N_2 and evaporation of KCl. It is not β-C_3N_4..

Table 6 The d-spacings(nm) of the crystallite found in CN_x film deposited on silicon substrate at 500°C, theoretical calculation of β-C_3N_4, silicon, and graphite

the crystal.	β-C_3N_4	silicon	graphite
	0.557		
0.483			
	0.322*	0.313	0.335
0.288	0.278*		
0.239			
0.219	0.221		
	0.211*		0.213
	0.193*	0.192	0.203
	0.186		
0.172	0.182*		0.180
	0.161	0.164	0.167
	0.158		
0.151	0.154*		0.154
0.143	0.147		
	0.139		
0.131	0.134	0.136	
0.122		0.124	

* high intensity ring

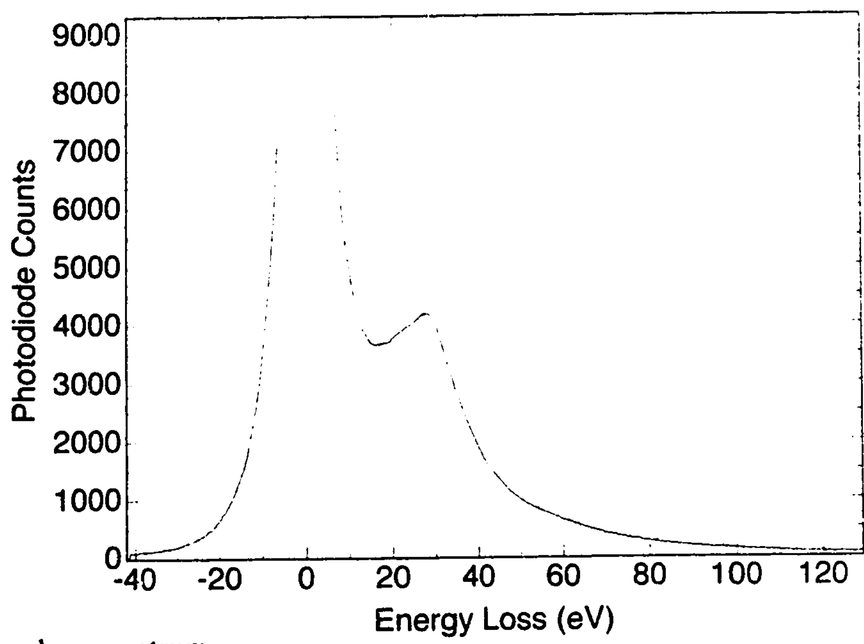

(a) low loss spectrum

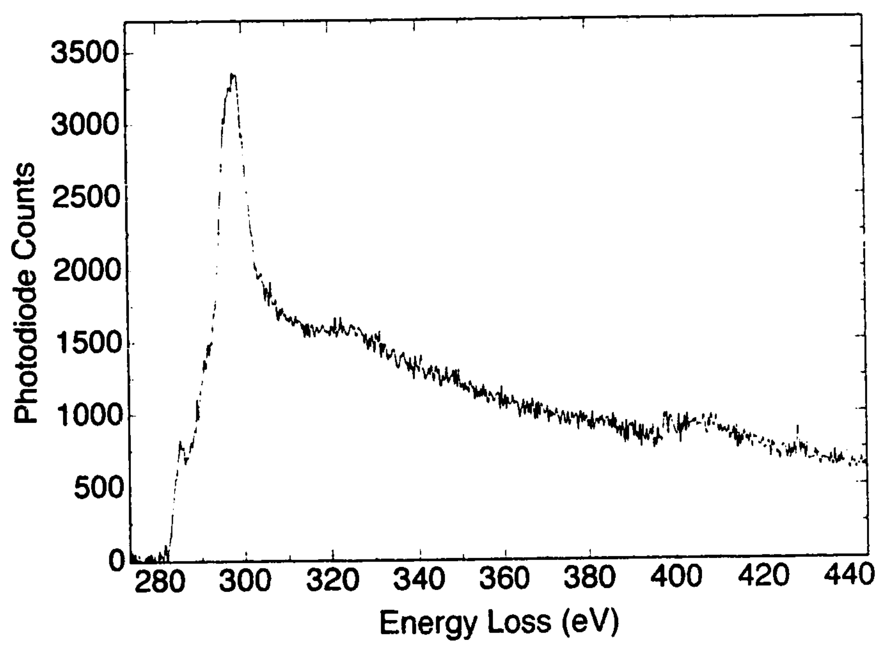

(b) K-shell loss spectrum

Fig. 21 Selected area EELS of the crystallite found in CN_x film deposited on silicon at 500°C

Chapter 5 CONCLUSIONS

The results in the previous chapter provide a picture of the composition and bond structure of CN_x films deposited by reactive carbon-arc evaporation and sputtering. The highest N/C ratio obtained by sputtering reached 0.75 when deposition was onto a mica substrate held at -100°C. Over 75% of the nitrogen was weakly bonded with carbon, and was easily released when annealed to 800°C. This weak bonding improved the electrical conductivity. Bombardment by carbon ions during deposition increases the fraction of C-N strong bonds. The fraction of sp^2 bonded electrons R_{sp2} of most CN_x films measured by carbon K-edge fine structure of EELS, was in excess of 100% and increased as nitrogen content increases. It cannot provide an accurate measure of the bond type because of the existence of other hybrids and charge transfer between nitrogen and carbon atoms. The same problem should exist in the Kramer-Kronig analysis and plasmon energy analysis of the low loss spectrum. In order to get exact values of the bond type in CN_x films by EELS, consideration of the charge transfer possibility is necessary. By transmission electron diffraction (TED) analysis, we found most of our samples to be predominantly amorphous, with no evidence of the predicted β-C_3N_4 phase in any sample.

BIBLIOGRAPHY

Berger,S.D., McKenzie, D.R. Martin, P.J. 1988, Philos. Mag. Lett., v57, p285

Bousetta, A., Lu, M., Bensaoula, A. and Schultz, a. 1994, Appl. Phys. Lett., v65, n6, p696

Bradley, D.E., 1954, British Journal of Applied Physics, v5, p65

Chen, M.Y., Lin, X., Dravid, V.P., Chung, Y.W., Wong, M.S. and Sproul, W.D., 1992, Surf. Coat. Technol., v54/55, p360

Chen, M.Y., Li, D., Lin, X., Dravid, V.P., Chung, Y., Wong, M., and Sproul, W.D., 1993, J. Vac. Sci. Technol., A11, p521

Cox, P.A., 1987, The electronic structure and chemistry of solid, Oxford University Press

Cuomo, J.J., Leary, P.A., Yu, D., Reuter, W., and Frisch, M., 1979, J.Vac. Sci. Technol., v16, p299

Davis, R.F.1992 ,Diamond Films and Coatings, Noyes Publications Press

Doll, G. L., Heremans, J. P., Perry, T. A., and Mantese, J.V., 1994, J. Mater. Res., v9, p85

Dworschak, W., et al 1990 Thin Solid Films, v189, p257 Fujimoto F., and Ogata, K., 1993, Jpn. J. Appl. Phys., v32, L420

Egerton, R.F. 1986, Electron Energy-loss Spectroscopy in the Electron Microscope, Plenum New York

Fallon, P.J. and Brown, L.M., 1993, Diamond and Related Material, v2, p1004

Fink, J., Muller-Heinzerling, T., Pfluger, J., Bubenzer, A., Koidl, P., and Crecelius, G, 1983, Solid State Communication, v47, n9, p687

Freire, F.L., Achete, C.A., Mariotto, G., and Canteri, R., 1994, J. Vac. Sci, Technol., A12, p3048

Fujimoto, F., and Ogata, K., 1990, Jpn. J. Appl. Phys., v32, L420

Han, H. and Feldman, B.J., 1988, Solid State Communications, v65, n9, p921

Hoffman, A., Gouzman, I., and Brener, R., 1993, Appl. Phys. Lett., v64, n7, p845

Jones, D.I. and Stewart, A.D., 1982, Philos. Mag., B46, p423

Kauffman, J.H. Metin, S., and Saperstein, D.D., 1989, Phys. Rev., B39, p13053

Kalish, R., Amir,.O., Brener, R.,Spits, R.A., and Derry, T.E., 1991, Appl. Phys., A52, p48

Li, D., Chung, Y-W., Wang, M., and Sproul, W.D., 1993, J. Appl. Phys., v74, n1, p219

Li, D., Chung, Y-W., Yang, S., Wong, M., Adibi, F., and Sproul, W.D., 1994, J. Vac. Sci. Technol., A12, p1470

Lin, S., Noonan, K., Feldman, B.J., Min, D., and Jones, M.T. 1991, Solid State Communications , v80, n2, p101

Liu, A.Y., and Cohen, M.L., 1989, Science, v245, p841

Liu, A.Y., and Cohen, M.L., 1990, Phys. Rev., B41, p10727

Liu. A.Y., and Wentzcovitch, R.M., 1994, Phys. Rev., B50, p10362

McLintock, I.S., and Orr, J.C., 1973, Physics and Chemistry of Carbon, v11, edited by P.L.Walker, New York: Dekker

Mansour, A., and Ugolini, D., 1993, Phys. Rev., B47, n16, p10201

Mariotto, G., and Freire, F.L., 1994, Thin Solid Films, v241, p255

Marton, D., Al-Bayati, A.H., Todorov, S.S., Boyd, K.J., and Rabalais, J.W., 1994, Nuclear Instrument and Methods in Physics Research, B90, p277

Marton, D. Boyd, K.J., Al-Bayati, A.H., Todorov, S.S, and Rabalais, J.W., 1994, Phys. Rev. Letts., v73, p118

Maya, L., Cole, D. R. and Hagaman, E. W. 1991, J. Am. Ceram. Soc., v74, n7, p1686

Meyerson, B. and Smith, F.W. 1980, Solid State Communications, v34 p531

Nakayama, N., Tsuchiya, Y., Tamada, S., Kosyge, K., Nagata, S., Takahiro, K., and Yamaguchi, S., 1993, Jpn. J. Appl. Phys., v32 L1465

Ning, X.J., Pirouz, P, Lagerlof, K.P.D. and Dicarlo, J., 1990, J. Mater. Res., v5, 2865

Niu, C., Yuan, Z., and Lieber, C.M., 1993, Science, v261, p334

Ogata, K., Chubaci, J.F.D., and Fujimoto, F., 1994, J. Appl. Phys., v76, p3791

Pinchas, S., and Laulicht, I., 1971, Infrared Spectra of Labelled Compounds, Academic, New York

Robertson, J., 1986, Adv. Phys., v35, p317

Rossi, F., Andre, B., Dunlop, H., Delplancke, M.P., and Hubbard, K., 1994, J. Mater. Res. v9, p2440

Sugai, I., Oyaizu, M., 1991, Nuclear Instruments and Methods in Physics Research, A303, p59

Sjostrom, H., Ivanov, I., Johansson, M., Hultman, L., Sundgren, J.-E., Hainsworth, S.V., Page, T.F., and Wallenberg, L.R., 1994, Thin Solid Films, v246, p103

Taft, E.A. and Philipp, H.R., 1965, Phys. Rev., v138, n1A, p197

Torng, C.J., Sivertsen, J.M., Judy, J.H., and Chang, C., 1990, J. Mater. Res., v5, n11, p2490

Veerasamy, V.S., Yuan, J., Gilkes, K.W.R., Weiler, M., and Brown, L.M. 1993 Phys. Rev. B48, p17954

Wang, Y., Chen, H.C., Hoffman, R.W., and Augus, J.C., 1990, J. Mater. Res., v5, p2378

Weissmantel, C. 1979, Thin Solid Films, v61, L5

Wixom, M.R., 1990 ,J. Am. Ceram. Soc., v73, p1973

Yeh, T., Lin, C., Siversen, J. M. and Judy, J.H., 1993 Journal of Magnetism and Magnetic Materials, v120, p314

Yu, K.M., Cohen M.L.,Haller, W.L., Liu, A.Y.,and Wu, I.C., 1994 Phys. Rew. B49, p5034

APPENDIX

The Fortran program for Kramers-Kronig analysis

```
C  Read in spectrum data
     DIMENSION D(2048), DI(2048)
     NN=1024
     MM=2*NN
     REALN=FLOAT(NN)
     OPEN(4, FILE='KK.DAT', STATUS='OLD')
     DO 10 IW=1,MM,10
   10 READ(4,*)D(IW),D(IW+2),D(IW+4),D(IW+6),D(IW+8)
     CLOSE(4)
C  Input the electron energy, ev/channel, collection semiangle
     E0=200
     EPC=0.3
     RI=1000
     BETA=11
     TGT=E0*(1022.12+E0)/(511.06+E0)
     SUM=0
C  Apply aperture correction APC
     DO 15 J=3,MM,2
     E=EPC*FLOAT(J-1)/2.
     APC=ALOG(1.+BETA*TGT/E)**2)
     D(J)=D(J)/APC
C Apply normalization factor RK
```

```
 15 SUM=SUM+D(J)/E
    RK=SUM/1.571/(1.-1./RI/RI)*EPC
    DO 17 J=1,MM,2
    D(J)=D(J)/RK
    DI(J)=D(J)
 17 D(J+1)=0
C Kramers-Kronig analysis
    CALL FFT(NN,+1,D)
    IM=2*NN-1
    DO 103 I=1,IM,2
    D(I)=-2.*D(I+1)/REALN
103 D(I+1)=0.
    DO 38 IR=1,NN,2
    D(NN+IR)=-D(NN+IR)
 38 CONTINUE
    CALL FFT(NN,-1,D)
    OPEN(4,FILE='FKK1.DAT',STATUS='OLD')
    WRITE(4,67)
 67 FORMAT(2X,'EV',16X,'RE',16X,'EPS1',16X,'EPS2')
    D1=D(1)
    DO 104 I=3,MM,2
    D(I)=D(I)+1.-D(NN-1)/2.*(FLOAT(NN-1)/FLOAT(2*NN-I))**2
    W=FLOAT((I-1)/2)*EPC + 0.0001
    DEN=D(I)*D(I)+DI(I)*DI(I)+0.0000001
    EPS1=D(I)/DEN
    EPS2=DI(I)/DEN
    WRITE(4,*)W,DI(I),EPS1,EPS2
104 CONTINUE
    CLOSE(4)
    STOP
```

```
      END
      SUBROUTINE FFT(NN,ISIGN,D)
      DIMENSION D(1034)
      N=2*NN
      J=1
      DO 5 I=1,N,2
      IF(I-J)1,2,2
    1 TR=D(J)
      TI=D(J+1)
      D(J)=D(I)
      D(J+1)=D(I+1)
      D(I)=TR
      D(I+1)=TI
    2 M=N/2
    3 IF(J-M)5,5,4
    4 J=J-M
      M=M/2
      IF(M-2)5,3,3
    5 J=J+M
      MM=2
    6 ML=MM-N
      IF(ML)7,10,10
    7 IS=2*MM
      TH=6.283185/FLOAT(ISIGN*MM)
      ST=SIN(TH/2)
      W1=-2.*ST*ST
      W2=SIN(TH)
      WR=1.
      WI=0.
      DO 9 M=1,MM,2
```

```
      DO 8 I=M,N,IS
      J=I+MM
      TR=WR*D(J)-WI*D(J+1)
      TI=WR*D(J+1)+WI*D(J)
      D(J)=D(I)-TR
      D(J+1)=D(I+1)-TI
      D(I)=D(I)+TR
    8 D(I+1)=D(I+1)+TI
      TR=WR
      WR=WR*W1-WI*W2+WR
    9 WI=WI*W1+TR*W2+WI
      MM=IS
      GO TO 6
   10 RETURN
      END
```